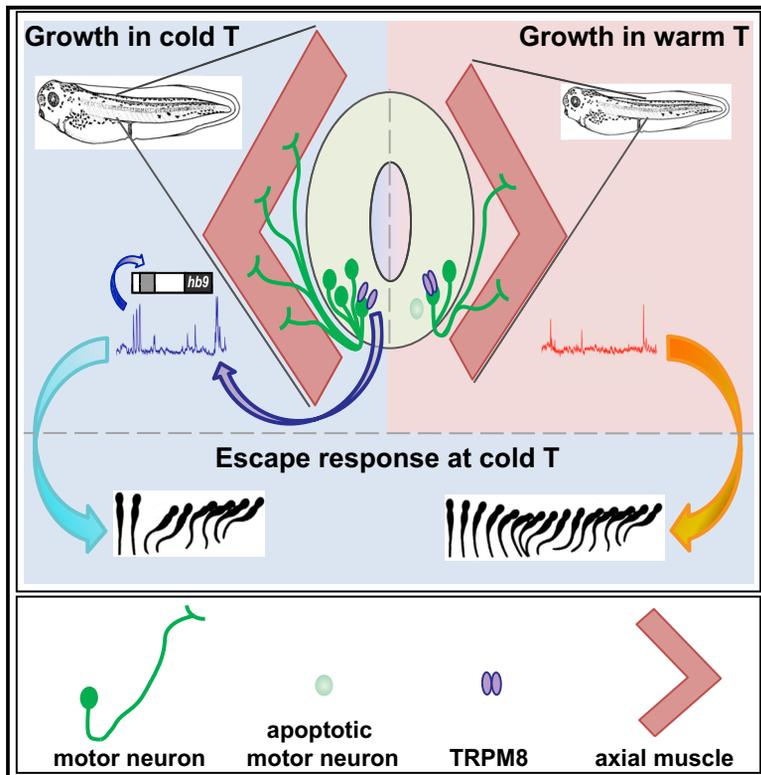# Current Biology

Growth at Cold Temperature Increases the Number of Motor Neurons to Optimize Locomotor Function

Graphical Abstract

Authors

Kira A. Spencer,
Yesser Hadj Belgacem, Olesya Visina,
Sangwoo Shim, Henry Genus,
Laura N. Borodinsky

Correspondence

lnborodinsky@ucdavis.edu

In Brief

Spencer et al. discover that *Xenopus* larvae reared in cold temperature are better equipped to escape upon touch at cold temperature relative to warm-grown siblings. This advantage is dependent on the cold-sensitive channel TRPM8, which is necessary for increased Ca^{2+} spike frequency in embryonic spinal neurons, their differentiation, and survival.

Highlights

- The environment regulates spinal cord development and sensorimotor function

- Cold temperature increases Ca^{2+} spike frequency in embryonic spinal cord neurons

- Motor neuron differentiation is dependent on environmental temperature and activity

- TRPM8 mediates cold-temperature-induced adapted phenotype of animals reared in cold

CellPress

Current Biology

Article

CellPress

Growth at Cold Temperature Increases the Number of Motor Neurons to Optimize Locomotor Function

Kira A. Spencer,[1] Yesser Hadj Belgacem,[1,2] Olesya Visina,[1] Sangwoo Shim,[1] Henry Genus,[1] and Laura N. Borodinsky[1,3,*]
[1]Department of Physiology & Membrane Biology and Institute for Pediatric Regenerative Medicine, Shriners Hospital for Children, University of California Davis School of Medicine, Sacramento, CA 95817, USA
[2]Present address: Institut de Neurobiologie de la Méditerranée (INMED), Institut National de la Santé et de la Recherche Médicale (INSERM), Parc Scientifique de Luminy, BP 13-13273, Marseille Cedex 09, France
[3]Lead Contact
*Correspondence: lnborodinsky@ucdavis.edu
https://doi.org/10.1016/j.cub.2019.04.072

SUMMARY

During vertebrate development, spinal neurons differentiate and connect to generate a system that performs sensorimotor functions critical for survival. Spontaneous Ca^{2+} activity regulates different aspects of spinal neuron differentiation. It is unclear whether environmental factors can modulate this Ca^{2+} activity in developing spinal neurons to alter their specialization and ultimately adjust sensorimotor behavior to fit the environment. Here, we show that growing *Xenopus laevis* embryos at cold temperatures results in an increase in the number of spinal motor neurons in larvae. This change in spinal cord development optimizes the escape response to gentle touch of animals raised in and tested at cold temperatures. The cold-sensitive channel TRPM8 increases Ca^{2+} spike frequency of developing ventral spinal neurons, which in turn regulates expression of the motor neuron master transcription factor HB9. TRPM8 is necessary for the increase in motor neuron number of animals raised in cold temperatures and for their enhanced sensorimotor behavior when tested at cold temperatures. These findings suggest the environment modulates neuronal differentiation to optimize the behavior of the developing organism.

INTRODUCTION

The spinal cord is essential for sensorimotor integration in vertebrates. During development, spinal neurons acquire specialized identities and form a network that carries out sensorimotor functions. Neural progenitors are specified through a sequential and combinatorial transcriptional program driven by intrinsic gradients of morphogenetic proteins along the dorsoventral and anteroposterior axis of the spinal cord [1]. Spontaneous electrical activity and early forms of neurotransmitter signaling further regulate different aspects of spinal neuron differentiation [2]. For instance, accelerating the developmental switch in the chloride gradient from depolarizing to hyperpolarizing, subsequent to

GABA or glycine receptor activation, decreases the number of spinal interneurons and motor neurons in the developing zebrafish [3]. In *Xenopus laevis* embryos, broadly manipulating spontaneous Ca^{2+} spike activity in spinal neurons, either pharmacologically or through ion channel overexpression, demonstrates that this activity regulates neurotransmitter specification in a homeostatic manner [4–6]. Spontaneous activity also regulates spinal neuron axon trajectory, another key feature of neuron functional identity, as observed for motor neurons in both chick and zebrafish embryos [7–9].

The numbers of mature, specialized spinal neurons are also dependent on the rate of apoptosis during development. For example, in chicken, mouse, and rat, 45%–90% of motor neurons undergo programmed cell death, depending on the species and the region of the developing spinal cord [10, 11]. Developmental motor neuron apoptosis is regulated by electrical activity [12] and trophic factors released by the innervated skeletal muscle [13].

To date, it is unclear what role environmental cues play in influencing spinal cord circuitry development, particularly whether these cues can modulate electrical activity during development, and in turn influence the neuron specialization and survival that are necessary to generate the circuits underlying sensorimotor function.

Xenopus laevis, an ectotherm whose body temperature is subject to fluctuations in environmental temperature, provides an ideal model to examine this problem. It is well established that temperature regulates the rate of embryonic and larval development in *Xenopus laevis* [14]. Furthermore, a phenomenon named the temperature-size rule, which holds that ectothermic animals reared in cold environmental temperatures have increased body size as adults [15], provides additional evidence that ectotherm development is susceptible to environmental perturbations. However, temperature's influence on nervous system development has not previously been studied.

Specifically, given that the spinal cord, and particularly motor neurons, develop and differentiate [16–20] during a critical period of spontaneous Ca^{2+} spike activity in embryonic spinal neurons [4, 5, 21–23], if the environment were to modify this activity it would potentially alter the functional features of developing neurons, eventually adapting the sensorimotor responses to the environment.

Here, we show that rearing *Xenopus laevis* embryos in cold temperature results in changes to spinal neuron specialization
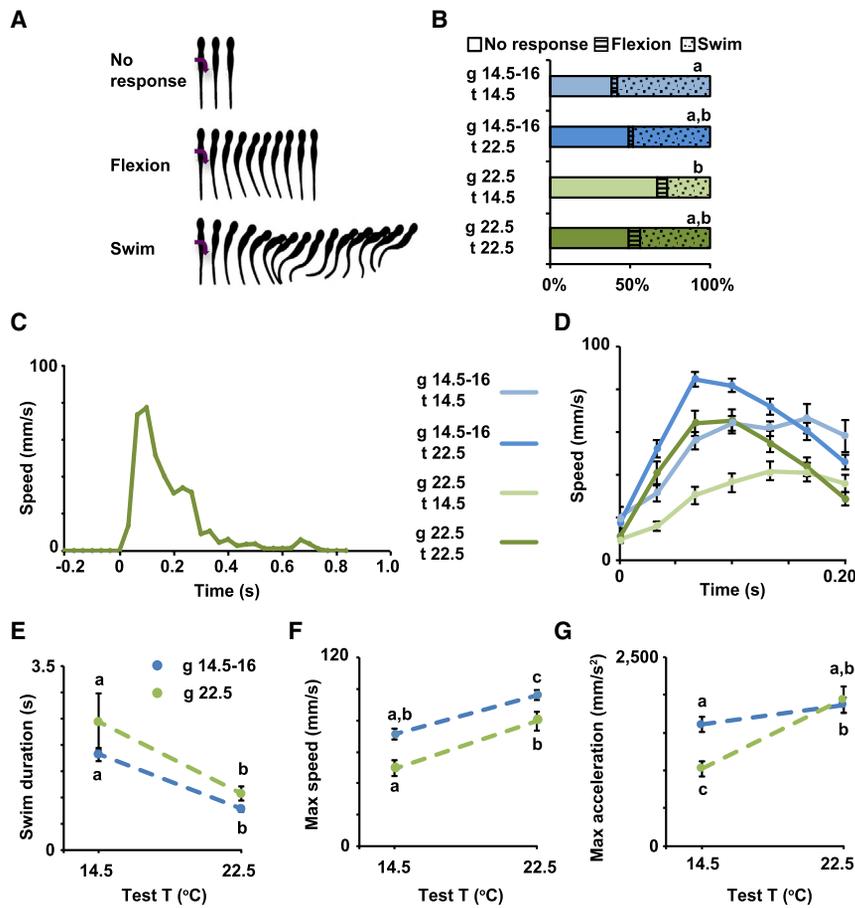
Figure 1. The Temperature of the Environment during Development Influences Early Swimming Behavior in *Xenopus laevis* Larvae

(A) Types of behavioral responses to gentle touch; modified from [26, 27].

(B–G) Stage 37/38 (B) and 40 (C-G) larvae grown in cold (blue, 14.5°C–16°C) or warm (green, 22.5°C) temperature were subjected to 20 trials each of gentle touch at cold (14.5°C) or warm (22.5°C) temperature. Responses were video recorded at 30 Hz, n = 6 larvae per condition.

(B) Average percentage of incidence of each response.

(C) Example of full time course of swim speed after gentle touch (0 s) from stage 40 larva grown in and tested at warm temperature.

(D) Time course of changes in speed during initial phase (first 200 ms) of the swim response.

(E) Swim duration.

(F) Maximum speed during initial phase of the swim response.

(G) Maximum tangential acceleration during initial phase of the swim response.

In (D)–(G), data are mean ± SEM. In (B) and (E)–(G), the letters on top of datasets indicate significant (different letters) or not significant (same letters) differences, p < 0.05, 2-way ANOVA, Tukey post hoc test.

See also Videos S1, S2, S3, and S4.

and survival, mediated by changes in Ca²⁺ spike activity, through recruiting the cold-sensitive channel TRPM8. The temperature-dependent changes in spinal cord development appear to optimize sensorimotor function of growing larvae to the environment.

RESULTS

Escape Swimming Is Enhanced in Larvae Grown in Cold Temperature

Non-amniotes such as amphibians and fishes lay their eggs in water, where embryos eventually hatch and continue developing their sensorimotor functions, all the while exposed to the external environment. To examine the influence of environmental temperature on the development of sensorimotor function of *Xenopus laevis*, we evaluated swimming responses to gentle touch during the early period after hatching in stage 37/38 and 40 larvae reared at either 14.5°C–16°C, on the low end of physiologically relevant environmental temperatures for this species, or 22.5°C, on the warm side of environmental temperatures for this species. Stage 37/38 larvae were chosen as an early developmental time point when larvae are static for the most part unless stimulated [24]. Stage 40 larvae were chosen as the endpoint in this study based on previous studies showing that different aspects of embryonic spontaneous activity-dependent neuronal differentiation are apparent at this developmental stage [5, 21, 22] and that the escape response to gentle touch be-

comes more robust, but not completely matured [25], suggesting potential for plasticity. *In vitro* fertilization was performed at room temperature, and, 4–5 h post-fertilization, stage 7–8 blastula were placed in their respective growth temperatures throughout the duration of development until their sensorimotor responses were assayed. Behavior of larvae from each growth temperature was assessed at both cold (14.5°C) and warm (22.5°C) temperatures, creating four experimental conditions. At stage 37/38, the sensorimotor responses elicited upon gentle touch include swimming away (Video S1), flexion (Video S2), or no response (Video S3; Figures 1A and 1B [26, 27]). We find a significant decrease in the incidence of swimming responses when assayed at cold temperature in animals raised in warm compared with animals raised in cold temperatures (Figure 1B), indicating that recently hatched larvae raised in cold temperature are more likely to elicit a simple escape response upon touch at cold temperature.

Following stage 37/38, motor neuron firing properties and muscle innervation patterns change to generate more mature swimming [24, 25]. At stage 40, we observed that the swimming response (Video S4) is characterized by an initial phase of rapid acceleration followed by a plateau at a maximum speed (Figures 1C and 1D). Although all the groups, regardless of growth and test temperatures, share these features, there are significant differences in the time course that characterizes the escape response in each group (Figure 1D). The first difference is between the groups tested at cold temperature compared to those tested at warm temperature; while larvae tested at warm temperature decelerate after reaching the initial plateau (Figures 1C

and 1D), larvae tested at cold temperature remain at maximum speed for at least 200 ms after the start of the response (Figure 1D). This difference may reflect constraints on how the neuromuscular system functions at different test temperatures. This shared relationship between larval behavior and test temperature is also evident in the average duration of the swimming response, which reveals that larvae swim for a longer time when tested at cold compared to warm temperatures regardless of the temperature in which they were raised (Figure 1E). It is important to note that swimming was tested in a relatively small dish (35-mm diameter), and that the interval between trials was relatively short ($\geq$ 5 s), both of which may impact swim duration. Larvae terminate swimming when sensory neurons in the head or cement gland are activated [28, 29], as reviewed by Roberts and colleagues [27], and this may occur when the larvae swim into the side of the dish. In addition, the short interval between trials may result in shorter episodes of swimming due to Na$^+$/K$^+$-pump-mediated membrane hyperpolarization [30]. It is then possible that the differences in swim duration found between test temperatures are associated with differences in the length of the refractory period at different test temperatures and/or the activation of the "stop signal" to terminate swimming may be sensitive to the test temperature.

Second, although the patterns of the speed curves are similar for groups tested at the same temperature, the maximum speed and acceleration are most similar among larvae tested in the temperature in which they were grown (Figures 1F and 1G), which suggests animals adapt to their growth temperature to perform in a stereotypic manner. Interestingly, larvae tested at temperatures that differ from their growth temperature reach maximum speed and acceleration that are either significantly higher or lower than animals grown and tested at the same temperature. Animals grown in cold but tested at warm temperature swim significantly faster than all other groups, indicating cold-grown animals outperform warm-grown animals in swimming away at warm temperature (Figures 1D and 1F). In contrast, animals grown in warm and tested at cold temperature swim the slowest and take the longest to reach maximum speed (Figures 1D and 1G). This indicates the efficiency of the response at cold temperature is diminished in animals grown in warmer temperatures, while those grown in cold temperatures show enhanced locomotor performance, demonstrating adaptation to the cold temperature condition. Altogether these data suggest that there is a significant interaction between the temperature in which animals are grown and the sensorimotor performance at different temperatures.

Spinal Motor Neuron Number Increases in Animals Grown in Cold Temperature

To investigate potential cellular mechanisms contributing to the temperature-dependent behavioral phenotypes, we assessed whether there are changes to the motor neuron population when animals are reared in cold versus warm temperatures. The motor neurons required for swimming in *Xenopus laevis* larvae are first generated during gastrulation and continue appearing until about stage 33/34 [16, 17], around the time larvae hatch. These motor neurons differentiate with axons innervating the axial skeletal muscle beginning around embryonic stage 25 [18, 19]. Motor neurons continue to differ-

entiate and mature as the embryos elongate and grow into free swimming larvae. Embryos were placed at the different temperatures beginning at blastula (stage 7–8) and allowed to develop until stage 40, encompassing the period of motor neuron birth, differentiation [18–20, 31], and, presumably, pruning as shown for other species [10, 11]. Staining for HB9, a transcription factor necessary for spinal motor neuron differentiation and maintenance [17, 32, 33], shows a 2-fold increase in the number of HB9-expressing cells in animals raised in cold temperature (14.5°C) compared to those raised in warm temperatures (22.5°C or 26.5°C, Figures 2A and 2B). This increase in HB9-expressing spinal neurons corresponds with an increase in the number of motor neurons retrogradely labeled from the ventral axial musculature in larvae grown at cold temperature compared to those grown at warmer temperatures (Figures 2C and 2D). Moreover, measurement of the area occupied by axons innervating the axial musculature reveals a higher motor neuron axonal density in animals raised in cold temperature (Figures 2E and 2F). Together, these data indicate there is an increase in the number of motor neurons in cold-grown animals.

In addition to the increase in motor neuron number, animals grown in cold temperature are on average about 10% longer compared to those grown in warm temperatures (Figure S1A), which correlates with 10% longer spacing between axonal tracts aligned along the chevrons of axial skeletal musculature (Figure S1B). There is also an increase in the thickness of the axial musculature in cold-grown animals compared to warm-grown animals (Figure S1C). These results show that animals grown at cold temperature exhibit an overall increase in the volume of axial musculature. Collectively, these data indicate that the cold-grown larvae are larger, consistent with the temperature-size rule in ectotherms, including temperature-size findings in *Xenopus laevis* metamorphs [15, 34].

Nevertheless, the considerable increase in the motor neuron number seen per unit length of the spinal cord suggests that specific cold-temperature-dependent rules might affect spinal neuron specialization and spinal cord development.

Apoptosis regulates cell number during development and could contribute to a change in larva size and spinal neuron numbers. In *Xenopus laevis*, apoptosis occurs as the spinal cord is forming [35, 36], but cold temperature is known to have a neuroprotective effect and can influence rates of apoptosis [37]. Motor neuron number peaks around stage 37/38 [38]; thus, we evaluated stage 40 larvae for subsequent apoptosis. We found that warm-grown animals show a higher number of apoptotic cells in the spinal cord compared with cold-grown animals, for which apoptotic spinal cells are barely apparent (Figures 2G and 2H). Moreover, within the motor neuron population approximately 30% of the HB9-expressing cells are TUNEL-positive in animals raised in warm temperature, while only less than 1% of the HB9-immunopositive cells are apoptotic when raised in cold temperature (Figures 2G and 2I). These results suggest that a decrease in the rate of apoptosis of spinal neurons in animals grown in cold temperature contributes to the increase in the number of motor neurons in animals grown in cold temperature (Figures 2A–2D).

Interestingly, developmentally regulated neuronal apoptosis is activity dependent [12], posing the possibility that
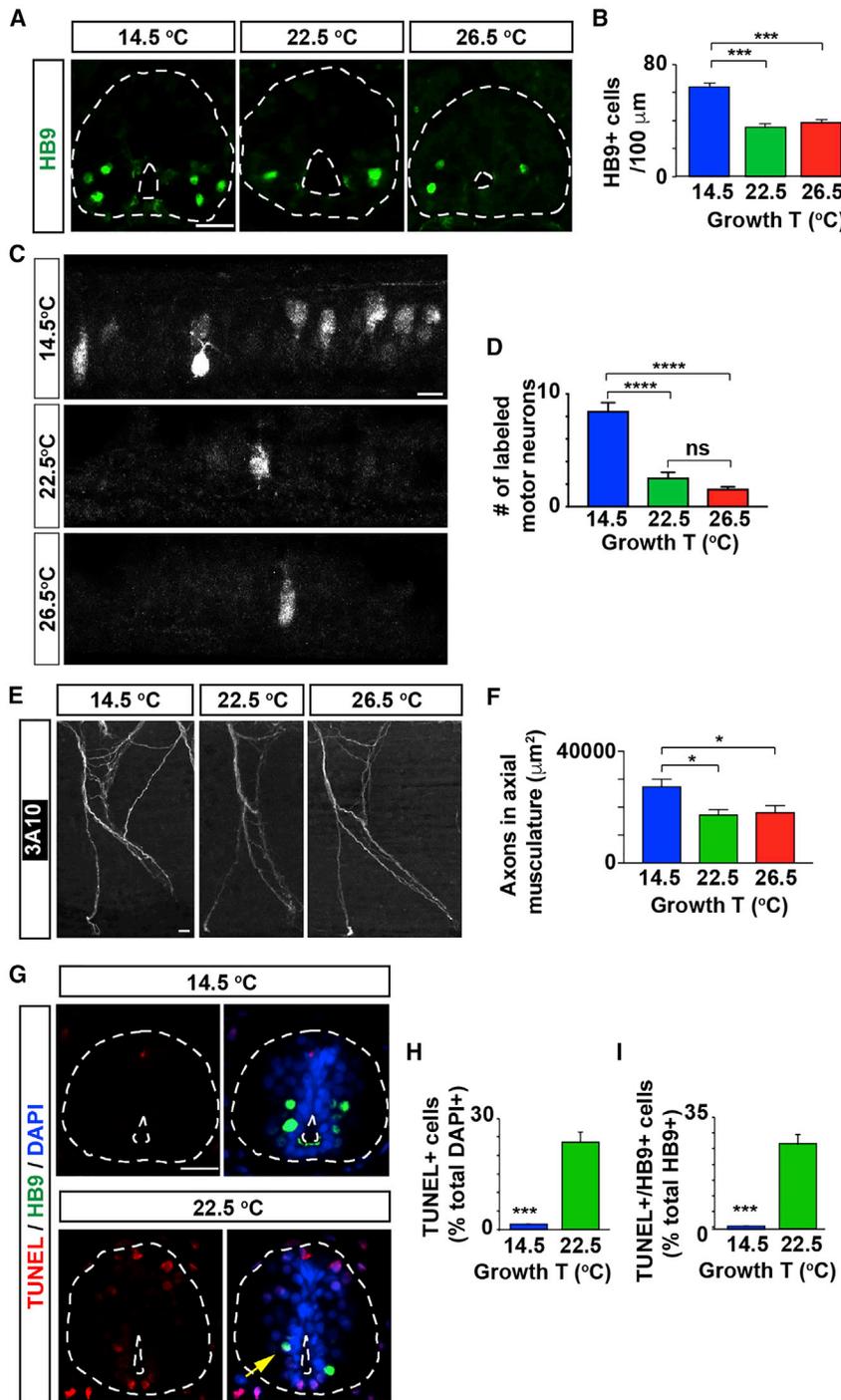
CellPress

Figure 2. The Number of Spinal Motor Neurons in Developing Larvae Is Temperature Dependent

(A) Images show cross-sections of immunostained spinal cord (outlined) from stage 40 larvae grown in cold (14.5°C) or warm (22.5 or 26.5°C) temperatures.

(B) Graph shows number of HB9-immunopositive cells per 100 μm of spinal cord; mean ± SEM from at least 220 μm length of spinal cord per larva, n ≥ 4 larvae per condition, ***$p < 0.001$, 1-way ANOVA, Tukey post hoc test.

(C) Images show maximum intensity projections of whole-mount spinal cord from stage 40 larvae grown in different temperatures followed by retrograde labeling with Alexa 488-dextran conjugate from ventral axial musculature.

(D) Graph shows numbers of retrogradely labeled motor neurons; mean ± SEM for each experimental group, n ≥ 10 larvae per condition, ****$p < 0.0001$; ns, not significant' Kruskal-Wallis test' Dunn's multiple comparisons test.

(E) Images show maximum intensity projections of whole-mount immunostained axonal bundle #5 (with 1 being the most anterior axonal bundle innervating the axial musculature) with the axonal marker 3A10 (neurofilament associated protein), from stage 40 larvae grown in the indicated temperatures.

(F) Graph shows area labeled per axonal bundles 4 through 7; mean ± SEM for each experimental group, n ≥ 10 larvae per condition, *$p < 0.05$, 1-way ANOVA, post hoc Tukey test.

(G–I) Larvae grown in cold temperature exhibit fewer apoptotic spinal cord cells and motor neurons.

(G) Images show cross-sections of immunostained spinal cord (outlined) from stage 40 larvae grown in different temperatures. Scale bars in (A), (C), (E), and (G), 20 μm.

(H and I) Graphs show percentage of TUNEL+ (H, per total DAPI-labeled nuclei) and HB9+/TUNEL+ cells (I, per total HB9+ cells) per 100 μm of spinal cord; mean ± SEM from at least 220 μm length of spinal cord per larva, n ≥ 4 larvae per condition, ***$p < 0.001$, two-tailed t test.

See also Figure S1.

Cold Temperature Increases Ca²⁺ Spike Frequency of Embryonic Ventral Spinal Neurons by Recruiting the Cold-Sensitive Channel TRPM8

In *Xenopus laevis,* there is a period of spontaneous Ca²⁺ activity in embryonic spinal neurons spanning from stage 20 to stage 28–30 [5, 22], corresponding with the stages when motor neurons differentiate [16–19]. To assess how environmental temperature acutely influences spontaneous Ca²⁺ spike activity during the period of neuronal differentiation [4, 5, 22, 23], we imaged embryonic spinal cord loaded with the cell-permeant Ca²⁺-sensitive dye Fluo4-AM. Ca²⁺ activity was recorded in the same sample at three different temperatures, 14.5°C, 22.5°C, and 26.5°C ± 0.5°C in a randomized order. We find that ventral spinal neurons, where

temperature-dependent control of different types of spinal neuron numbers may be regulated by neuronal activity. Moreover, previous studies have established an important role for spontaneous Ca²⁺ activity in neuronal phenotype specification [4–6, 39–41]. We hypothesize that environmental factors such as temperature modify the pattern of spontaneous activity, which in turn, regulate the numbers of specialized spinal neurons to generate the most appropriate neural network to operate within the constraints of the environmental conditions.
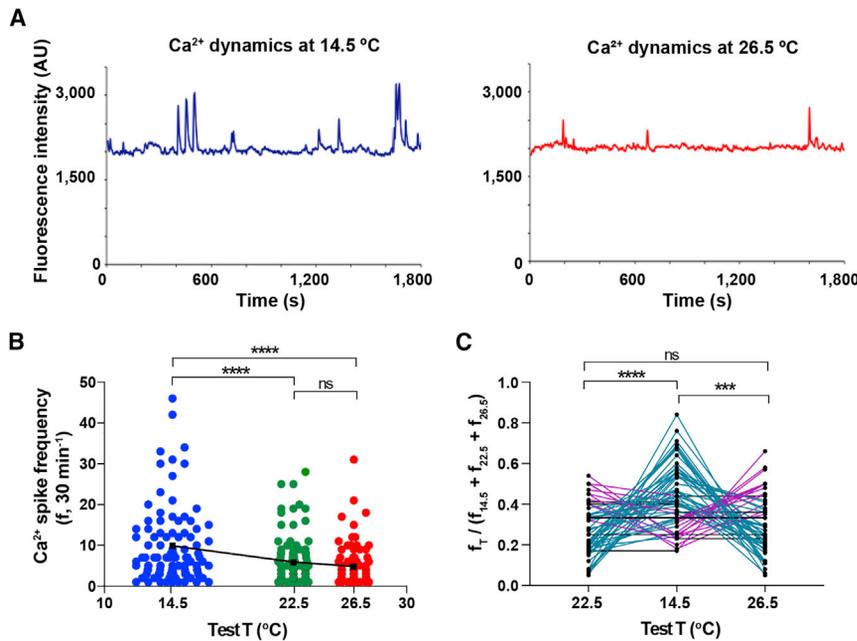
Figure 3. Cold Temperature Acutely Increases Ca^{2+} Spike Frequency of Embryonic Ventral Spinal Neurons

Ventral view of spinal cords from stage 24 embryos were Ca^{2+} imaged for 30-min intervals at 14.5°C, 22.5°C, and 26.5°C ± 0.5°C, in a randomized order.

(A) Traces illustrate the same representative ventral spinal neuron imaged at the indicated temperatures.

(B) Graph shows individual cell and mean (black squares) Ca^{2+} spike frequency (30 min^{-1}) from N = 4 ventral spinal cords (n of neurons analyzed: 14.5°C, 102; 22.5°C, 104; 26.5°C, 86), ****p < 0.0001; ns, not significant; repeated-measures mixed effect analysis; post hoc Tukey test.

(C) Graph shows ratio of Ca^{2+} spikes at each temperature compared to the sum of spikes at the 3 temperatures per cell, n = 58. Teal lines represent neurons with higher spike frequency at 14.5°C, magenta lines represent neurons with higher spike frequency at 22.5°C or 26.5°C, and black lines represent neurons with no change in spike frequency across temperatures; ***p < 0.001, ****p < 0.0001; ns, not significant; repeated-measures 2-way ANOVA, post hoc Tukey test.

developing motor neurons are located, exhibit a significantly higher Ca^{2+} spike frequency at cold temperature compared to the frequencies at warmer temperatures (Figures 3A and 3B). A closer comparison of the relative frequencies for those individual ventral spinal neurons showing Ca^{2+} spike activity at all three temperatures reveals that a high proportion of cells (~65%) displayed a significantly higher spike frequency at 14.5°C (teal lines) relative to 22.5°C and 26.5°C (Figure 3C).

The transient receptor potential cation channel subfamily M member 8, TRPM8, is the main detector of environmental cold by sensory neurons [42–44]. The *Xenopus laevis* genome contains two copies of *trpm8* (*trpm8* and *trpm8b*); however, only TRPM8 responds to cold temperatures [45, 46]. Previous work has found TRPM8 in primary afferent neurons of juvenile *Xenopus laevis* frogs [45]. More recent RNA sequencing (RNA-seq) data in embryonic and larval stages show that *trpm8* transcript levels peak at stage 25 and is enriched in neural tissue [47], suggesting that TRPM8 may play a role during embryonic development beyond its function in dorsal root ganglia in the mature nervous system. Indeed, we find by RT-PCR that *trpm8* transcripts are present in whole-embryo samples, as well as in the embryonic spinal cord (Figures 4A, S3A, and S3B), before dorsal root ganglia develop [48]. *In situ* hybridization further demonstrates specific expression of *trpm8* in the brain and spinal cord of stage 24 embryos (Figure 4B), when spontaneous Ca^{2+} spike activity is apparent in spinal neurons. Western blot assays and immunostaining identify TRPM8 protein is expressed throughout development, including the stages when spontaneous Ca^{2+} spike activity manifests (Figures 4C, 4D, S2A, S2B, S2D, and S3D–S3H). The TRPM8 antibody (validated through expression of TRPM8 in a heterologous system [49]) appears to recognize specifically *Xenopus laevis* TRPM8 at a band between 100 and 150 kDa, which consistently decreases when knockdown approaches are implemented by injecting either of two non-overlapping translation-blocking TRPM8-targeted mor-

pholinos (TRPM8-tbMO1 and 2; Figures 4C, S2A, S2D, S3D, S3F, and S3G) and that increases in optical density when TRPM8 is overexpressed (Figures S2A and S3H). Moreover, immunostained transverse spinal cord sections from unilaterally TRPM8 overexpressing embryos show enhanced signal from the TRPM8 antibody in the affected half spinal cord (Figure S2B). However, the antibody also binds to what appear to be non-specific bands of lower molecular weight than predicted for *Xenopus laevis* TRPM8 protein (132 [naked]-150 [glycosylated] kDa [50]) and for which their optical density does not change consistently with the manipulations of TRPM8 protein expression (Figures S3D–S3H). Immunostaining in transverse sections reveals TRPM8 is expressed in the embryonic spinal cord and enriched in ventral spinal neurons (Figures 4D and S2B), where an increase in Ca^{2+} spike frequency is apparent at cold temperature (Figure 3). Moreover, assessment of functional expression of TRPM8 in the embryonic spinal cord by acute addition of (−)-menthol reveals that this TRPM8 agonist elicits Ca^{2+} transients in ventral spinal neurons (Figure 4E).

The temperature for *X. laevis* TRPM8 half-maximal activation is 13.9°C [45], suggesting that, at the test temperature of 14.5°C used in this study, this channel should be activated. To assess whether TRPM8 participates in the cold-temperature-dependent increase in Ca^{2+} spike frequency in embryonic ventral spinal neurons, we incubated exposed ventral spinal cords with the TRPM8 inhibitor N-(3-Aminopropyl)-2-[(3-methylphenyl)methoxy]-N-(2-thienylmethyl)benzamide hydrochloride (AMTB [51]) and compared the acute changes in activity when switching from 26.5°C, where *X. laevis* TRPM8 remains mostly closed, to 14.5°C, where TRPM8 activity is expected [45, 51]. Our results indicate that inhibiting TRPM8 reverses the effect of switching from 26.5°C to 14.5°C observed in vehicle-treated control samples (Figure 4F). In the presence of AMTB, the majority of neurons (~86%) exhibit a decrease in Ca^{2+} spike frequency when switched from 26.5°C to 14.5°C,
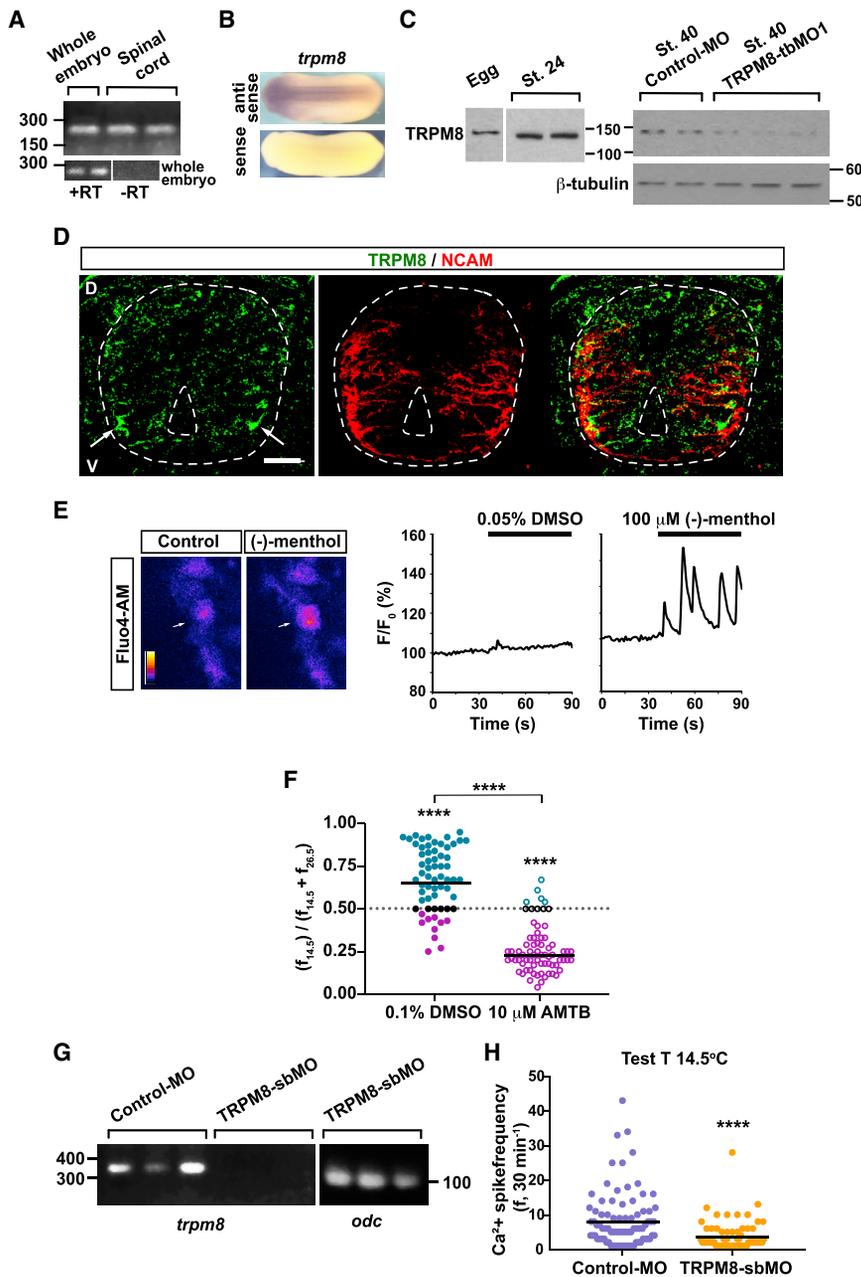
Figure 4. TRPM8 Is Necessary for the Cold-Temperature-Mediated Increase in Ca²⁺ Spike Frequency in the Ventral Spinal Cord

(A) RT-PCR for *trpm8* (236 bp) from cDNA extracted from stage 24 whole embryo or dissected spinal cord. +/−RT, in the presence or absence of the reverse transcriptase, respectively, during conversion of isolated mRNA into cDNA.

(B) *In situ* hybridization for *trpm8* in stage 24 embryos showing specific labeling in brain and spinal cord.

(C) Western blot assays from egg, stage 24 wild-type whole embryo or from stage 40 whole larva, control morpholino (MO) or TRPM8-translation-blocking MO 1 (TRPM8-tbMO1) lysates. Predicted TRPM8 molecular weight [MW]: 132 kDa. Shown are representative examples of one of 3 independent experiments. β-tubulin was used as loading control.

(D) Immunostained transverse section of stage 25 spinal cord (outlined). D, dorsal; V, ventral; scale bar, 20 μm; arrows indicate TRPM8 clusters in ventral neuron domains. NCAM labeling was used as counterstaining.

(E) Stage 24 ventral spinal cord from wild-type embryos was Ca²⁺ imaged at 1 Hz for 90 s. Either 100 μM (−)-menthol or vehicle (0.05% DMSO) was added after 35 s of imaging and recording continued for another 60 s. Images show a menthol-responsive ventral neuron before (left, control) and after (right) addition of (−)-menthol. Colored scale shows fluorescence intensity in arbitrary units. Traces show the changes in fluorescence for the indicated cell (arrow) in both trials.

(F) Stage 24 ventral spinal cord from wild-type embryos was Ca²⁺ imaged in 30-min intervals at cold (14.5°C) and warm (26.5°C) temperatures in the absence (vehicle, 0.1% DMSO) or presence of 10 μM AMTB, TRPM8 inhibitor. Scatterplots show changes in Ca²⁺ spike frequency when switching temperatures in individual spinal neurons and geometric mean (black lines) from N = 3 ventral spinal cords per condition (n of neurons analyzed: DMSO, 62; AMTB, 71). Teal circles represent neurons with higher spike frequency at 14.5°C, magenta circles represent neurons with higher spike frequency at 26.5°C, and black circles represent neurons with no change in spike frequency across temperatures; ****p < 0.0001, comparison within treatments Wilcoxon matched-pairs signed rank, two-tailed test.

(G) RT-PCR from cDNA collected from stage 46 larvae previously injected with 2.5 pmol standard control morpholino (Control-MO) or TRPM8-splicing-blocking morpholino (TRPM8-sbMO) shows that *trpm8* mature transcript (349 bp) is not detected in TRPM8-sbMO animals. *odc*: ornithine decarboxylase (101 bp) as positive control.

(H) TRPM8-sbMO or Control-MO containing spinal cord from stage 24 embryos were Ca²⁺-imaged for 30 min at cold temperature (14.5°C). Graph shows individual (scatterplots) and geometric mean (black lines) Ca²⁺ spike frequency from N = 3 ventral spinal cords per group (n of neurons analyzed: Control-MO, 81; TRPM8-sbMO, 64), ****p < 0.001, Kolmogorov-Smirnov, two-tailed test.

See also Figures S2 and S3.

rather than the increase observed in the majority (~74%) of vehicle-treated control neurons (Figures 4F and S2C). Although a recent study shows that AMTB also inhibits human voltage-gated sodium channels [52], because our results only demonstrate a change in spike frequency at cold temperature, we suggest AMTB acts specifically at TRPM8 to decrease the spike frequency in *Xenopus* ventral spinal neurons. This may

be due to the fact that functional expression of voltage-gated sodium channels is low at these developmental stages in the embryonic spinal cord [53], which correlates with the predominance of Ca²⁺-dependent, long-duration action potentials that later in development transition to the brief sodium-dependent counterparts [54, 55] characteristic of the mature nervous system.
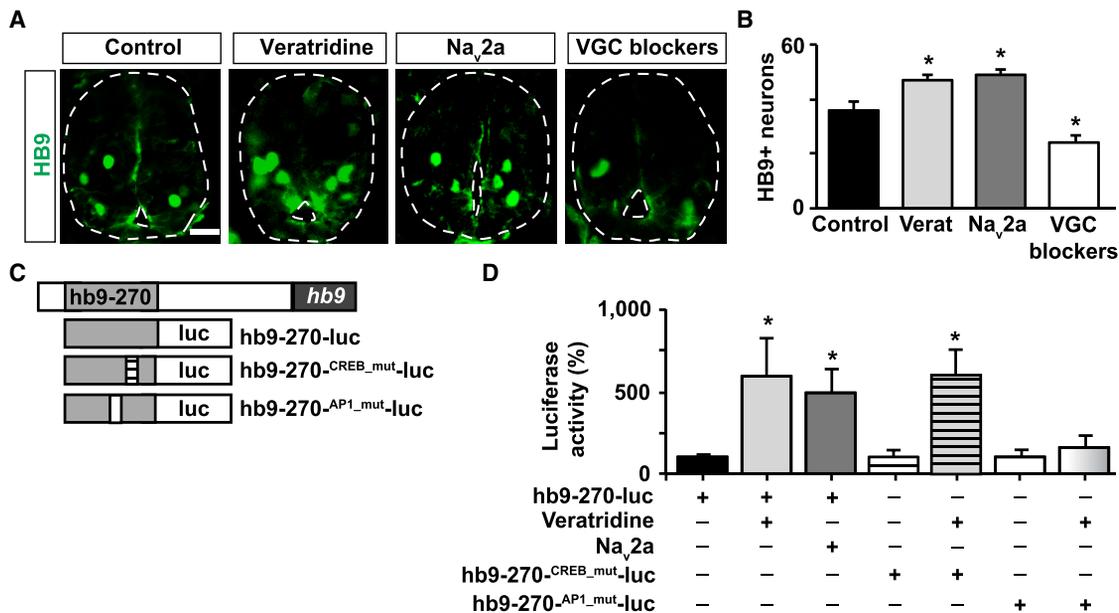
CellPress

Figure 5. Electrical Activity Regulates the Number of Motor Neurons in the Spinal Cord and *hb9* Transcription

(A) Images show cross-sections of immunostained spinal cord (outlined) from stage 35 larvae in which activity was enhanced (veratridine [verat], Na_v2a over-expression) or suppressed (voltage-gated Na^+ and Ca^{2+} channel blockers [VGC blockers]: calcicludine, ω-conotoxin-GVIA, flunarizine, and tetrodotoxin). Scale bar, 20 μm

(B) Graph shows number of HB9-immunopositive cells per 100 μm spinal cord; mean ± SEM from at least 220 μm length of spinal cord per larva, $n \geq 4$ larvae per condition, *$p < 0.05$, 1-way ANOVA.

(C) Schematic of luciferase reporters used to assess regulation of *hb9* transcription. Gray box represents a 270-bp fragment from the M250/Region B in the *hb9* 5' regulatory region.

(D) Spinal cord from wild-type or Na_v2a-overexpressing embryos injected with wild-type or mutant forms of the *hb9* transcription reporter were incubated for 8 h with 1 μM veratridine or vehicle only and processed for luciferase activity measurements. Graph shows percentage of normalized luciferase intensity compared with control (wild-type embryo incubated with vehicle only), mean ± SEM, n > 5 spinal cords per group, *$p < 0.05$, 1-way ANOVA.

To further investigate the role of TRPM8 in *Xenopus* spinal cord development, we knocked down TRPM8 expression by injecting 2-cell stage embryos with either a splice-blocking (TRPM8-sbMO) or a translation-blocking morpholino (TRPM8-tbMO1). Similar to the pharmacological approach, knockdown of TRPM8 with TRPM8-sbMO (Figures 4G and S3C) reveals average spike frequencies at cold temperature that are significantly lower than in control-MO-containing neurons (Figure 4H). Moreover, we observed that, when TRPM8 is knocked down with TRPM8-tbMO1 (Figures S2D and S3D), there is a loss of cold-temperature-dependent increase in Ca^{2+} spike frequency in TRPM8-deficient embryonic ventral spinal neurons compared with wild-type counterparts (Figure S2E).

Altogether these results demonstrate that the pattern of spontaneous Ca^{2+} activity in embryonic spinal neurons is sensitive to the environmental temperature and that recruitment of temperature-sensitive channels, like TRPM8, contributes to temperature-specific patterns of Ca^{2+}-mediated electrical activity. Alongside the observed temperature-dependent change in motor neuron number (Figure 2), these findings suggest a temperature-mediated, Ca^{2+} signaling-dependent mechanism for motor neuron specification and survival.

Activity-Dependent Motor Neuron Differentiation

To determine whether motor neuron differentiation is activity dependent, both pharmacological and genetic approaches

were used to modulate Ca^{2+} spike activity during a critical period in spinal neuron differentiation [4, 5, 22, 23]. When activity was enhanced either by implanting beads impregnated with the Na_v channel agonist veratridine or through overexpression of the voltage-gated Na^+ channel, Na_v2a [4, 5, 21, 23], motor neuron numbers increased compared to control (Figures 5A and 5B). Conversely, when Ca^{2+} spike activity was suppressed with Ca^{2+} and Na^+ channel blockers [4, 5, 21, 23], motor neuron numbers decreased (Figures 5A and 5B).

To further investigate a potential Ca^{2+} signaling-dependent mechanism regulating motor neuron specification, we searched for activity-responsive elements in the *HB9* regulatory region that could respond to modulations in electrical activity/Ca^{2+} signaling. We found two potential activity-responsive elements (CRE-like and AP1) in the 5' regulatory region of the human *HB9* gene in a region conserved across species called M250 or region B. This region is capable of controlling HB9 expression in mouse and chicken [56, 57]. We sub-cloned a 270-bp fragment containing these activity-responsive elements and placed it directly upstream of a gene coding for firefly luciferase (Figure 5C). Enhancing Ca^{2+} spike activity by either overexpressing Na_v2a in the spinal cord or by incubating dissected spinal cord with veratridine increases luciferase signal (Figure 5D). Mutating the CRE-like sequence had no effect on the activity-induced increase in luciferase signal. In contrast, mutating the putative AP1 site abolished this effect (Figure 5D).
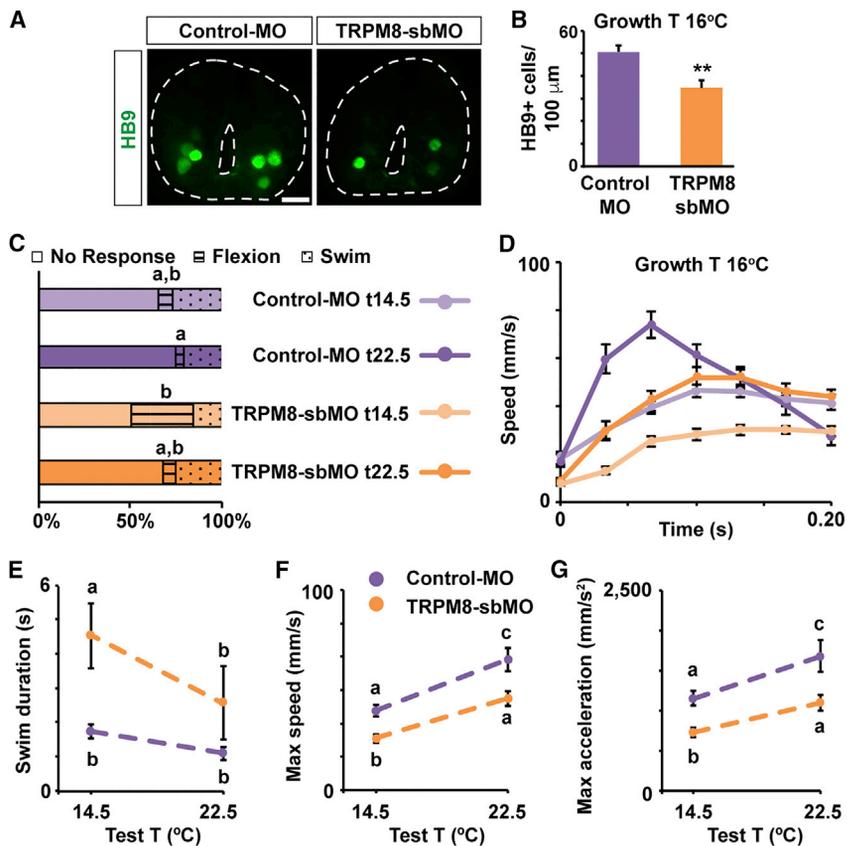
Figure 6. TRPM8 Is Necessary for the Increase in Motor Neuron Number and the Adaptation of the Sensorimotor Response of Animals Grown in Cold Temperatures

(A) Images show cross-sections of immunostained spinal cord (outlined) for HB9 from Control-MO- or TRPM8-sbMO-containing stage 40 larvae grown in cold temperature (16°C). Scale bar, 20 μm.

(B) Graph shows number of HB9-immunopositive cells per 100 μm of spinal cord; mean ± SEM from at least 220 μm-length spinal cord per larva, n = 5 larvae per condition, **p < 0.005, two-tailed t test.

(C–G) TRPM8-sbMO or Control-MO stage 37/38 (C) and 40 (D–G) larvae grown in cold temperature (16°C) were subjected to 20 trials each of gentle touch at cold (14.5°C) or warm (22.5°C) temperature. Responses were video recorded at 30 Hz, n = 6 larvae per condition.

(C) Average percentage of incidence of each response.

(D) Time course of changes in speed during initial phase (first 200 ms) of the swim response.

(E) Swim duration.

(F) Maximum speed during initial phase of the swim response.

(G) Maximum tangential acceleration during initial phase of the swim response.

In (D)–(G), data are mean ± SEM. In (C) and (E)–(G), the letters on top of datasets indicate significant (different letters) or not significant (same letters) differences, p < 0.05, 2-way ANOVA, Tukey post hoc test.

See also Video S5.

These results indicate that electrical activity participates in the specification of motor neurons by transcriptionally regulating HB9 expression in developing spinal neurons.

TRPM8 Is Necessary for the Increase in Motor Neuron Number and Optimized Sensorimotor Performance in Cold-Grown Animals

Because TRPM8 mediates the cold-temperature-induced increase in Ca^{2+} spike frequency of embryonic ventral spinal neurons, and Ca^{2+} activity promotes motor neuron specification, we then assessed whether TRPM8 function is necessary for the increased number of motor neurons when animals are raised in cold temperatures. Results show that animals grown in cold temperature that are deficient in TRPM8 exhibit lower numbers of HB9-immunopositive neurons compared to controls (Figures 6A and 6B). The number of motor neurons in TRPM8-deficient animals grown in cold temperatures is instead comparable to wild-type animals grown in warm temperatures (cf. Figures 2A and 2B with Figures 6A and 6B).

This led us to ask whether animals deficient in TRPM8, thus experiencing warm-temperature levels of Ca^{2+} activity and lower number of motor neurons while raised in cold temperature, maintain the improvement in swimming behavior seen in wild-type animals raised in and tested at cold temperature. To address this, we knocked down TRPM8 expression throughout development, grew animals in cold temperature, and assessed escape swimming in these larvae and control counterparts (Figures 6C–6G).

Examining the response rates to light touch indicates there is a difference in the initiation and completion of the escape response in TRPM8-deficient larvae compared with Control-MO siblings. Although there was no significant change in the incidence of swim responses at either stage 37/38 or stage 40, TRPM8-sbMO larvae tested at cold temperature exhibit more flexion responses (Figure 6C). In addition, by stage 40 larvae deficient in TRPM8 swam for a significantly longer period of time at cold temperature than any other treatment group (Figure 6E) and exhibited phases of slowing-down followed by speeding-up again and continuing to swim, unlike the other groups that terminated swimming after a single response cycle (Video S5).

Results show that the phases of the speed-time curve from Control-MO larvae tested at warm and cold temperature are comparable with those from uninjected, wild-type larvae grown in cold temperature (cf. Figures 1D with 6D). In contrast, TRPM8-deficient larvae tested at cold temperature are the slowest and have the lowest maximum acceleration of all the experimental groups (Figures 6D, 6F, and 6G). This phenotype resembles the uninjected larvae grown in warm and tested at cold temperature (Figures 1D, 1F, and 1G) and suggests that larvae deficient in TRPM8 fail to develop optimized sensorimotor behavioral traits at cold temperature despite growing in cold temperature. Moreover, the shape of the speed-time curve for TRPM8-sbMO larvae tested at warm temperature is most similar to the curve for Control-MO
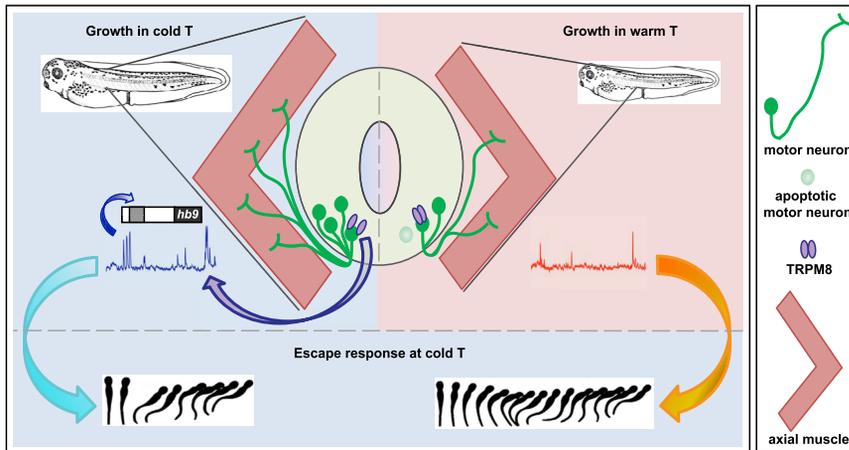
Figure 7. Model of Mechanism of Cold-Temperature Adaptation

TRPM8 activation at cold temperature results in an increase in Ca^{2+} spike frequency in developing spinal cord neurons. This enhanced spike frequency increases HB9-dependent motor neuron differentiation and survival. The low-temperature mediated increase in motor neuron number facilitates faster escape swimming at cold temperature compared to animals grown in warm temperature, for efficiently evading predators and increasing rate of survivability.

larvae tested at cold temperature (Figure 6D). Strikingly, this is reminiscent of the relationship between uninjected animals grown and tested at cold and those grown and tested at warm temperature (Figure 1D), even though both Control-MO- and TRPM8-sbMO-injected animals were grown in cold temperature.

Overall, these findings demonstrate TRPM8 is necessary for developing escape responses that are adapted to cold-temperature growth conditions.

DISCUSSION

Development of sensorimotor function is crucial for the viability of organisms across species. For anamniotes, in particular, a properly functioning sensorimotor system enables them to escape from potential danger, such as predators or an adverse environmental condition, during early development. Here, we discover that *Xenopus* embryos grown in cold temperature develop into larvae that are better equipped to escape upon touch at cold temperature compared to embryos grown in warm temperature. This advantage is dependent on the cold-sensitive channel TRPM8, which is necessary for the increased spontaneous Ca^{2+} spike activity that embryonic ventral spinal neurons exhibit when exposed to cold temperature. In turn, this enhanced activity promotes the specification and survival of the motor neuron phenotype, ultimately contributing to a higher number of motor neurons in animals grown in cold temperatures. Altogether, our results support a model in which an increase in the number of motor neurons contributes to improved escape swimming at cold temperatures in animals grown in cold temperatures, compared to animals grown in warm temperatures (Figure 7).

The numbers of motor neurons and motor units animals are able to establish have a direct impact on locomotor performance. For instance, during zebrafish development, dopaminergic signaling from the brainstem to the spinal cord promotes the specification of spinal motor neurons. Inhibiting this signaling leads to a reduction in motor neuron numbers and impaired motor responses in swimming larvae [58]. TRPM8 knockdown abrogates the cold-temperature-dependent increase in spontaneous activity and results in both a decrease in motor neuron numbers and impaired locomotor performance at cold temperatures,

despite growing in cold temperatures. This suggests that the increase in motor neuron numbers in wild-type animals grown in cold temperatures may function to enhance larval locomotor performance at cold temperatures.

We provide evidence for an activity-dependent mechanism regulating motor neuron number. Our experiments indicate *hb9* expression and the number of HB9$^+$ neurons increase when activity is enhanced. Previous studies have established HB9 is required for specifying and maintaining the motor neuron phenotype, including, in many species, axon pathfinding necessary for muscle innervation [32, 33, 59]. Furthermore, in chicken and zebrafish, motor neuron axon morphology is activity dependent [7, 9]. The increased spontaneous activity in developing ventral spinal neurons at cold temperature, described in this study, may change the pattern of muscle innervation.

Moreover, the interdependence of muscle and motor neuron growth and survival during development and disease has been established through many pioneering studies [60, 61]. The size of the motor neuron pool that innervates the axial musculature may also change with the concomitant enlargement of the muscle in animals grown at cold temperatures. The observed increase in muscle volume in cold-grown animals could be due to either an increase in number of muscle fibers or an increase in the size of the individual muscle fibers, or both. It may be that more motor neurons are required to innervate an increase in muscle fiber number or size. Thus, in future studies it would be interesting to determine this relationship and explore potential consequences. For instance, an increase in muscle fiber number could contribute to the decrease in apoptosis observed in motor neurons of cold-grown animals.

The cold temperature can be seen as a challenging environmental condition when assessed from the perspective of motor function. Isolated muscle fibers at cold temperatures exhibit less efficient metabolism, meaning they consume more oxygen to achieve the same mechanical force compared with muscle performing at warmer temperatures [62, 63]. Muscles are stiffer; thus, the same stimulus elicits weaker contractility at cold temperatures, and the contraction-relaxation cycles are slower [64]. Moreover, acclimating animals to cold temperature does not significantly modify the poor performance of skeletal muscle fibers at cold temperature [63, 65]. Despite this, animals grown at cold temperature seem to overcome these challenges to muscle performance in cold temperatures [65] and exhibit a sensorimotor response and locomotor activity that is on par with their

siblings grown and tested at room temperature, as demonstrated in this study. While we present data supporting a mechanism that involves cold-temperature-dependent regulation of motor neuron number that in turn facilitates the locomotor response at cold temperature, further work is required to gain an understanding of where additional temperature-dependent changes in the sensorimotor integration process are manifest. For instance, whether changes occur in the mechanosensory pathway controlling swim initiation or in the central pattern generator output that drives swimming remains to be investigated. Recording neuronal activity during fictive swimming from animals grown at different temperatures would provide insight into changes in these pathways. For example, the pattern of activity in spinal ventral roots, which underlie swimming, matures from stage 37/38 to stage 42 to better control swim direction and speed [24, 25]. Future studies may reveal that maturation of these important contributing components to the sensorimotor function is also sensitive to the temperature in which animals grow.

In addition, numbers and function of other neuronal types might also be sensitive to environmental temperature and may contribute to adapted sensorimotor behavior. For instance, the mid-hindbrain reticulospinal neurons are a population of GABAergic interneurons important for terminating the swim response in hatchling larvae as well as keeping larvae at rest in the absence of an environmental threat [66–69]. While the escape response is essential for evading impending threats in the environment, keeping still to prevent drawing the attention of potential predators is another key survival trait in hatchling larvae [70]. When TRPM8 is knocked down, larvae exhibit abnormal patterns of initiating and completing the swim response, which suggests TRPM8 expression during development may impact neuronal populations mediating these aspects of the escape responses.

Future studies exploring neurotransmitter phenotype expression might also provide further insight into mechanisms for regulating temperature-dependent changes in the sensorimotor system. Previous studies have established the number of *Xenopus laevis* spinal neurons expressing inhibitory or excitatory neurotransmitters is sensitive to broad changes in Ca^{2+} spike frequency [4–6]. These activity-dependent changes in neurotransmitter phenotype expression include the motor neuron population, both in the developing *Xenopus* spinal cord [21] and in the adult zebrafish subjected to exercise or spinal cord injury [71]. Nonetheless, unlike earlier studies where Ca^{2+} activity was modified throughout the entire spinal cord [4–6, 21, 23], the higher Ca^{2+} spike frequency at cold temperature reported in this study is restricted to about 60%–70% of ventral spinal neurons. Thus, it would be interesting to examine what changes occur to neurotransmitter phenotype in embryos reared at cold temperature when the activity of only a subset of spinal neurons is affected.

Evidence that temperature-sensitive channels are also expressed during mammalian development suggests the potential for temperature-dependent intervention in neural development is shared among both ectotherms and endotherms. In mammals, TRPM8 is also expressed embryonically, even before thermoregulation is established [72]. Likewise, warm and hot-temperature-sensitive channels are expressed early in development.

Specifically, the temperature-sensitive channels TRPV1 and TRPV2 are expressed in the mouse embryo with the latter detected in both developing dorsal root ganglia neurons as well as in motor neurons [73]. Work in young postnatal (P0–P3) mice indicates both TRPM8 and TRPV1 afferent activation modulates spinal motor networks [74]. Furthermore, TRPV2 channel activity is important for a cation current that regulates motor neuron properties in 1-week-old mice [75]. Because expression of temperature-sensitive ion channels is not restricted to adult sensory neurons, changes in temperature may have an impact on neural activity during nervous system development as shown in this study. Indeed, activation of TRPV4 by a modest increase in temperature in mouse neonate hippocampal neurons changes their excitability and maturation [76, 77]. Additionally, in humans, the risk of autism spectrum disorder in children born to mothers who experienced febrile episodes during pregnancy is increased according to several epidemiological studies [78–80] and diminished by antipyretic medications [80].

We conclude that physiological changes in temperature modify nervous system development in *Xenopus laevis* and suggest temperature may potentially impact nervous system development in many species, including humans. Overall, this study supports the idea that the *Xenopus laevis* nervous system develops to optimize swimming performance to the water temperature experienced during growth. Testing sensorimotor behavior reveals a significant interaction between the temperature in which an animal is grown and the temperature at which the test is performed. Animals reared in warm temperature accelerate and swim slower when placed at a cold temperature. However, cold-grown animals accelerate and swim just as fast at the cold temperature as the warm-temperature-grown animals tested at warm temperature. This suggests there is a homeostatic target toward which the neuromuscular system develops, so that escape swim speeds reach a certain magnitude in the temperature matching the growth temperature. Robustness and stereotypical performance under different temperatures is apparent in other systems as well, like in the pyloric circuit of the crab stomatogastric ganglion [81–83] or in *Aplysia*'s accessory radula closer neuromuscular system [84]. Furthermore, when cold-temperature detection is disrupted during development by knocking down TRPM8 expression, cold-grown animals no longer maintain this improved swimming performance at the cold temperature. This indicates TRPM8 expression and subsequent cold-temperature detection is required to mediate the developmental changes, which allow the sensorimotor system to function optimally in the cold temperature.

STAR★METHODS

Detailed methods are provided in the online version of this paper and include the following:

- KEY RESOURCES TABLE
- CONTACT FOR REAGENT AND RESOURCE SHARING
- EXPERIMENTAL MODEL AND SUBJECT DETAILS
  - Frog embryo and larva growth conditions
- METHOD DETAILS
  - Sensorimotor behavior
  - Immunostaining

CellPress

- ○ Retrograde labeling of motor neurons
- ○ TUNEL (Terminal deoxynucleotidyl transferase dUTP nick end labeling) assay
- ○ Calcium imaging
- ○ Manipulation of spontaneous Ca^{2+} activity
- ○ Luciferase Assay
- ○ RT-PCR
- ○ *In situ* hybridization
- ○ Western blot assays
- ○ TRPM8 knockdown
- ○ TRPM8 overexpression
- ● QUANTIFICATION AND STATISTICAL ANALYSIS
  - ○ Statistical analysis

SUPPLEMENTAL INFORMATION

Supplemental Information can be found online at https://doi.org/10.1016/j.cub.2019.04.072.

AUTHOR CONTRIBUTIONS

K.A.S. and L.N.B. designed the full scope of this study; Y.H.B. and L.N.B. designed the experiments related with the activity-dependent specification of motor neurons and HB9 expression. K.A.S. executed fully or partially all the experiments presented in this study and analyzed all the data presented. Y.H.B. executed the experiments related to activity-dependent motor neuron specification and HB9 transcription and analyzed the data obtained from those experiments. O.V. contributed to the data on TUNEL assay and HB9 expression in TRPM8-sbMO and Control-MO larvae and on RT-PCR and TRPM8 overexpression experiments. S.S. contributed to the design of TRPM8-sbMO experiments and *in situ* hybridization assays. L.N.B. contributed with retrograde labeling of motor neurons and menthol calcium imaging experiments. H.G. contributed to the analysis of behavioral experiments. K.A.S. and L.N.B. wrote the paper.

DECLARATION OF INTERESTS

The authors declare no competing interests.

REFERENCES

1. Yamada, T., Pfaff, S.L., Edlund, T., and Jessell, T.M. (1993). Control of cell pattern in the neural tube: motor neuron induction by diffusible factors from notochord and floor plate. Cell *73*, 673–686.

2. Borodinsky, L.N., Belgacem, Y.H., and Swapna, I. (2012). Electrical activity as a developmental regulator in the formation of spinal cord circuits. Curr. Opin. Neurobiol. *22*, 624–630.

3. Reynolds, A., Brustein, E., Liao, M., Mercado, A., Babilonia, E., Mount, D.B., and Drapeau, P. (2008). Neurogenic role of the depolarizing chloride gradient revealed by global overexpression of KCC2 from the onset of development. J. Neurosci. *28*, 1588–1597.

4. Belgacem, Y.H., and Borodinsky, L.N. (2011). Sonic hedgehog signaling is decoded by calcium spike activity in the developing spinal cord. Proc. Natl. Acad. Sci. USA *108*, 4482–4487.

5. Borodinsky, L.N., Root, C.M., Cronin, J.A., Sann, S.B., Gu, X., and Spitzer, N.C. (2004). Activity-dependent homeostatic specification of transmitter expression in embryonic neurons. Nature *429*, 523–530.

6. Marek, K.W., Kurtz, L.M., and Spitzer, N.C. (2010). cJun integrates calcium activity and tlx3 expression to regulate neurotransmitter specification. Nat. Neurosci. *13*, 944–950.

7. Hanson, M.G., and Landmesser, L.T. (2004). Normal patterns of spontaneous activity are required for correct motor axon guidance and the expression of specific guidance molecules. Neuron *43*, 687–701.

8. Kastanenka, K.V., and Landmesser, L.T. (2013). Optogenetic-mediated increases in in vivo spontaneous activity disrupt pool-specific but not dorsal-ventral motoneuron pathfinding. Proc. Natl. Acad. Sci. USA *110*, 17528–17533.

9. Plazas, P.V., Nicol, X., and Spitzer, N.C. (2013). Activity-dependent competition regulates motor neuron axon pathfinding via PlexinA3. Proc. Natl. Acad. Sci. USA *110*, 1524–1529.

10. Hamburger, V. (1975). Cell death in the development of the lateral motor column of the chick embryo. J. Comp. Neurol. *160*, 535–546.

11. Yamamoto, Y., and Henderson, C.E. (1999). Patterns of programmed cell death in populations of developing spinal motoneurons in chicken, mouse, and rat. Dev. Biol. *214*, 60–71.

12. Banks, G.B., Choy, P.T., Lavidis, N.A., and Noakes, P.G. (2003). Neuromuscular synapses mediate motor axon branching and motoneuron survival during the embryonic period of programmed cell death. Dev. Biol. *257*, 71–84.

13. Oppenheim, R.W., Haverkamp, L.J., Prevette, D., McManaman, J.L., and Appel, S.H. (1988). Reduction of naturally occurring motoneuron death in vivo by a target-derived neurotrophic factor. Science *240*, 919–922.

14. Nieuwkoop, P.D., and Faber, J. (1994). Normal Table of Xenopus laevis (Daudin): A Systematical and Chronological Survey of the Development from the Fertilized Egg till the End of Metamorphosis (Garland).

15. Angilletta, M.J., Jr., Steury, T.D., and Sears, M.W. (2004). Temperature, growth rate, and body size in ectotherms: fitting pieces of a life-history puzzle. Integr. Comp. Biol. *44*, 498–509.

16. Lamborghini, J.E. (1980). Rohon-beard cells and other large neurons in *Xenopus* embryos originate during gastrulation. J. Comp. Neurol. *189*, 323–333.

17. Saha, M.S., Miles, R.R., and Grainger, R.M. (1997). Dorsal-ventral patterning during neural induction in Xenopus: assessment of spinal cord regionalization with xHB9, a marker for the motor neuron region. Dev. Biol. *187*, 209–223.

18. van Mier, P., van Rheden, R., and ten Donkelaar, H.J. (1985). The development of the dendritic organization of primary and secondary motoneurons in the spinal cord of Xenopus laevis. An HRP study. Anat. Embryol. (Berl.) *172*, 311–324.

19. van Mier, P., Armstrong, J., and Roberts, A. (1989). Development of early swimming in *Xenopus laevis* embryos: myotomal musculature, its innervation and activation. Neuroscience *32*, 113–126.

20. Hartenstein, V. (1993). Early pattern of neuronal differentiation in the Xenopus embryonic brainstem and spinal cord. J. Comp. Neurol. *328*, 213–231.

21. Borodinsky, L.N., and Spitzer, N.C. (2007). Activity-dependent neurotransmitter-receptor matching at the neuromuscular junction. Proc. Natl. Acad. Sci. USA *104*, 335–340.

22. Root, C.M., Velázquez-Ulloa, N.A., Monsalve, G.C., Minakova, E., and Spitzer, N.C. (2008). Embryonically expressed GABA and glutamate drive electrical activity regulating neurotransmitter specification. J. Neurosci. *28*, 4777–4784.

23. Swapna, I., and Borodinsky, L.N. (2012). Interplay between electrical activity and bone morphogenetic protein signaling regulates spinal neuron differentiation. Proc. Natl. Acad. Sci. USA *109*, 16336–16341.

CellPress

24. Zhang, H.Y., Issberner, J., and Sillar, K.T. (2011). Development of a spinal locomotor rheostat. Proc. Natl. Acad. Sci. USA *108*, 11674–11679.

25. Sillar, K.T., Wedderburn, J.F., and Simmers, A.J. (1991). The development of swimming rhythmicity in post-embryonic Xenopus laevis. Proc. Biol. Sci. *246*, 147–153.

26. Boothby, K.M., and Roberts, A. (1995). Effects of site of tactile stimulation on the escape swimming responses of hatchling Xenopus laevis embryos. J. Zool. *235*, 113–125.

27. Roberts, A., Li, W.C., and Soffe, S.R. (2010). How neurons generate behavior in a hatchling amphibian tadpole: an outline. Front. Behav. Neurosci. *4*, 16.

28. Boothby, K.M., and Roberts, A. (1992). The stopping response of Xenopus laevis embryos: behaviour, development and physiology. J. Comp. Physiol. A Neuroethol. Sens. Neural Behav. Physiol. *170*, 171–180.

29. Roberts, A., and Blight, A.R. (1975). Anatomy, physiology and behavioural rôle of sensory nerve endings in the cement gland of embryonic xenopus. Proc. R. Soc. Lond. B Biol. Sci. *192*, 111–127.

30. Zhang, H.Y., and Sillar, K.T. (2012). Short-term memory of motor network performance via activity-dependent potentiation of Na+/K+ pump function. Curr. Biol. *22*, 526–531.

31. Hartenstein, V. (1989). Early neurogenesis in Xenopus: the spatio-temporal pattern of proliferation and cell lineages in the embryonic spinal cord. Neuron *3*, 399–411.

32. Arber, S., Han, B., Mendelsohn, M., Smith, M., Jessell, T.M., and Sockanathan, S. (1999). Requirement for the homeobox gene Hb9 in the consolidation of motor neuron identity. Neuron *23*, 659–674.

33. Thaler, J., Harrison, K., Sharma, K., Lettieri, K., Kehrl, J., and Pfaff, S.L. (1999). Active suppression of interneuron programs within developing motor neurons revealed by analysis of homeodomain factor HB9. Neuron *23*, 675–687.

34. Walsh, P.T., Downie, J.R., and Monaghan, P. (2008). Temperature-mediated morphology changes during metamorphic climax in the African clawed frog, Xenopus laevis. J. Therm. Biol. *33*, 244–249.

35. Hensey, C., and Gautier, J. (1998). Programmed cell death during Xenopus development: a spatio-temporal analysis. Dev. Biol. *203*, 36–48.

36. Estabel, J., Mercer, A., König, N., and Exbrayat, J.-M. (2003). Programmed cell death in Xenopus laevis spinal cord, tail and other tissues, prior to, and during, metamorphosis. Life Sci. *73*, 3297–3306.

37. Yenari, M.A., and Han, H.S. (2012). Neuroprotective mechanisms of hypothermia in brain ischaemia. Nat. Rev. Neurosci. *13*, 267–278.

38. Roberts, A., Walford, A., Soffe, S.R., and Yoshida, M. (1999). Motoneurons of the axial swimming muscles in hatchling Xenopus tadpoles: features, distribution, and central synapses. J. Comp. Neurol. *411*, 472–486.

39. Demarque, M., and Spitzer, N.C. (2010). Activity-dependent expression of Lmx1b regulates specification of serotonergic neurons modulating swimming behavior. Neuron *67*, 321–334.

40. Dulcis, D., and Spitzer, N.C. (2008). Illumination controls differentiation of dopamine neurons regulating behaviour. Nature *456*, 195–201.

41. Dulcis, D., and Spitzer, N.C. (2012). Reserve pool neuron transmitter respecification: Novel neuroplasticity. Dev. Neurobiol. *72*, 465–474.

42. Bautista, D.M., Siemens, J., Glazer, J.M., Tsuruda, P.R., Basbaum, A.I., Stucky, C.L., Jordt, S.E., and Julius, D. (2007). The menthol receptor TRPM8 is the principal detector of environmental cold. Nature *448*, 204–208.

43. Colburn, R.W., Lubin, M.L., Stone, D.J., Jr., Wang, Y., Lawrence, D., D'Andrea, M.R., Brandt, M.R., Liu, Y., Flores, C.M., and Qin, N. (2007). Attenuated cold sensitivity in TRPM8 null mice. Neuron *54*, 379–386.

44. Dhaka, A., Murray, A.N., Mathur, J., Earley, T.J., Petrus, M.J., and Patapoutian, A. (2007). TRPM8 is required for cold sensation in mice. Neuron *54*, 371–378.

45. Myers, B.R., Sigal, Y.M., and Julius, D. (2009). Evolution of thermal response properties in a cold-activated TRP channel. PLoS ONE *4*, e5741.

46. Saito, S., and Shingai, R. (2006). Evolution of thermoTRP ion channel homologs in vertebrates. Physiol. Genomics *27*, 219–230.

47. Session, A.M., Uno, Y., Kwon, T., Chapman, J.A., Toyoda, A., Takahashi, S., Fukui, A., Hikosaka, A., Suzuki, A., Kondo, M., et al. (2016). Genome evolution in the allotetraploid frog Xenopus laevis. Nature *538*, 336–343.

48. van Mier, P., and ten Donkelaar, H.J. (1988). The development of primary afferents to the lumbar spinal cord in Xenopus laevis. Neurosci. Lett. *84*, 35–40.

49. Toro, C.A., Eger, S., Veliz, L., Sotelo-Hitschfeld, P., Cabezas, D., Castro, M.A., Zimmermann, K., and Brauchi, S. (2015). Agonist-dependent modulation of cell surface expression of the cold receptor TRPM8. J. Neurosci. *35*, 571–582.

50. Dragoni, I., Guida, E., and McIntyre, P. (2006). The cold and menthol receptor TRPM8 contains a functionally important double cysteine motif. J. Biol. Chem. *281*, 37353–37360.

51. Lashinger, E.S., Steiginga, M.S., Hieble, J.P., Leon, L.A., Gardner, S.D., Nagilla, R., Davenport, E.A., Hoffman, B.E., Laping, N.J., and Su, X. (2008). AMTB, a TRPM8 channel blocker: evidence in rats for activity in overactive bladder and painful bladder syndrome. Am. J. Physiol. Renal Physiol. *295*, F803–F810.

52. Yapa, K.T.D.S., Deuis, J., Peters, A.A., Kenny, P.A., Roberts-Thomson, S.J., Vetter, I., and Monteith, G.R. (2018). Assessment of the TRPM8 inhibitor AMTB in breast cancer cells and its identification as an inhibitor of voltage gated sodium channels. Life Sci. *198*, 128–135.

53. O'Dowd, D.K., Ribera, A.B., and Spitzer, N.C. (1988). Development of voltage-dependent calcium, sodium, and potassium currents in Xenopus spinal neurons. J. Neurosci. *8*, 792–805.

54. Spitzer, N.C., and Lamborghini, J.E. (1976). The development of the action potential mechanism of amphibian neurons isolated in culture. Proc. Natl. Acad. Sci. USA *73*, 1641–1645.

55. Spitzer, N.C., and Baccaglini, P.I. (1976). Development of the action potential in embryo amphibian neurons in vivo. Brain Res. *107*, 610–616.

56. Lee, S.K., Jurata, L.W., Funahashi, J., Ruiz, E.C., and Pfaff, S.L. (2004). Analysis of embryonic motoneuron gene regulation: derepression of general activators function in concert with enhancer factors. Development *131*, 3295–3306.

57. Nakano, T., Windrem, M., Zappavigna, V., and Goldman, S.A. (2005). Identification of a conserved 125 base-pair Hb9 enhancer that specifies gene expression to spinal motor neurons. Dev. Biol. *283*, 474–485.

58. Reimer, M.M., Norris, A., Ohnmacht, J., Patani, R., Zhong, Z., Dias, T.B., Kuscha, V., Scott, A.L., Chen, Y.C., Rozov, S., et al. (2013). Dopamine from the brain promotes spinal motor neuron generation during development and adult regeneration. Dev. Cell *25*, 478–491.

59. Odden, J.P., Holbrook, S., and Doe, C.Q. (2002). Drosophila HB9 is expressed in a subset of motoneurons and interneurons, where it regulates gene expression and axon pathfinding. J. Neurosci. *22*, 9143–9149.

60. McLennan, I.S. (1988). Quantitative relationships between motoneuron and muscle development in Xenopus laevis: implications for motoneuron cell death and motor unit formation. J. Comp. Neurol. *271*, 19–29.

61. McLennan, I.S. (1982). Size of motoneuron pool may be related to number of myotubes in developing muscle. Dev. Biol. *92*, 263–265.

62. Koga, S., Wüst, R.C., Walsh, B., Kindig, C.A., Rossiter, H.B., and Hogan, M.C. (2013). Increasing temperature speeds intracellular PO2 kinetics during contractions in single Xenopus skeletal muscle fibers. Am. J. Physiol. Regul. Integr. Comp. Physiol. *304*, R59–R66.

63. Seebacher, F., Tallis, J.A., and James, R.S. (2014). The cost of muscle power production: muscle oxygen consumption per unit work increases at low temperatures in Xenopus laevis. J. Exp. Biol. *217*, 1940–1945.

64. James, R.S., Tallis, J., Herrel, A., and Bonneaud, C. (2012). Warmer is better: thermal sensitivity of both maximal and sustained power output in the iliotibialis muscle isolated from adult Xenopus tropicalis. J. Exp. Biol. *215*, 552–558.

65. Wilson, R.S., James, R.S., and Johnston, I.A. (2000). Thermal acclimation of locomotor performance in tadpoles and adults of the aquatic frog Xenopus laevis. J. Comp. Physiol. B *170*, 117–124.

66. Perrins, R., Walford, A., and Roberts, A. (2002). Sensory activation and role of inhibitory reticulospinal neurons that stop swimming in hatchling frog tadpoles. J. Neurosci. *22*, 4229–4240.

67. Li, W.C., Perrins, R., Walford, A., and Roberts, A. (2003). The neuronal targets for GABAergic reticulospinal inhibition that stops swimming in hatchling frog tadpoles. J. Comp. Physiol. A Neuroethol. Sens. Neural Behav. Physiol. *189*, 29–37.

68. Lambert, T.D., Li, W.C., Soffe, S.R., and Roberts, A. (2004). Brainstem control of activity and responsiveness in resting frog tadpoles: tonic inhibition. J. Comp. Physiol. A Neuroethol. Sens. Neural Behav. Physiol. *190*, 331–342.

69. Roberts, A., Dale, N., Ottersen, O.P., and Storm-Mathisen, J. (1987). The early development of neurons with GABA immunoreactivity in the CNS of Xenopus laevis embryos. J. Comp. Neurol. *261*, 435–449.

70. Lambert, T.D., Howard, J., Plant, A., Soffe, S., and Roberts, A. (2004). Mechanisms and significance of reduced activity and responsiveness in resting frog tadpoles. J. Exp. Biol. *207*, 1113–1125.

71. Bertuzzi, M., Chang, W., and Ampatzis, K. (2018). Adult spinal motoneurons change their neurotransmitter phenotype to control locomotion. Proc. Natl. Acad. Sci. USA *115*, E9926–E9933.

72. Takashima, Y., Ma, L., and McKemy, D.D. (2010). The development of peripheral cold neural circuits based on TRPM8 expression. Neuroscience *169*, 828–842.

73. Shibasaki, K., Murayama, N., Ono, K., Ishizaki, Y., and Tominaga, M. (2010). TRPV2 enhances axon outgrowth through its activation by membrane stretch in developing sensory and motor neurons. J. Neurosci. *30*, 4601–4612.

74. Mandadi, S., Nakanishi, S.T., Takashima, Y., Dhaka, A., Patapoutian, A., McKemy, D.D., and Whelan, P.J. (2009). Locomotor networks are targets of modulation by sensory transient receptor potential vanilloid 1 and transient receptor potential melastatin 8 channels. Neuroscience *162*, 1377–1397.

75. Bouhadfane, M., Tazerart, S., Moqrich, A., Vinay, L., and Brocard, F. (2013). Sodium-mediated plateau potentials in lumbar motoneurons of neonatal rats. J. Neurosci. *33*, 15626–15641.

76. Shibasaki, K., Suzuki, M., Mizuno, A., and Tominaga, M. (2007). Effects of body temperature on neural activity in the hippocampus: regulation of resting membrane potentials by transient receptor potential vanilloid 4. J. Neurosci. *27*, 1566–1575.

77. Shibasaki, K., Tominaga, M., and Ishizaki, Y. (2015). Hippocampal neuronal maturation triggers post-synaptic clustering of brain temperature-sensor TRPV4. Biochem. Biophys. Res. Commun. *458*, 168–173.

78. Atladóttir, H.O., Henriksen, T.B., Schendel, D.E., and Parner, E.T. (2012). Autism after infection, febrile episodes, and antibiotic use during pregnancy: an exploratory study. Pediatrics *130*, e1447–e1454.

79. Wilkerson, D.S., Volpe, A.G., Dean, R.S., and Titus, J.B. (2002). Perinatal complications as predictors of infantile autism. Int. J. Neurosci. *112*, 1085–1098.

80. Zerbo, O., Iosif, A.M., Walker, C., Ozonoff, S., Hansen, R.L., and Hertz-Picciotto, I. (2013). Is maternal influenza or fever during pregnancy associated with autism or developmental delays? Results from the CHARGE (CHildhood Autism Risks from Genetics and Environment) study. J. Autism Dev. Disord. *43*, 25–33.

81. Haddad, S.A., and Marder, E. (2018). Circuit Robustness to Temperature Perturbation Is Altered by Neuromodulators. Neuron *100*, 609–623.

82. O'Leary, T., and Marder, E. (2016). Temperature-Robust Neural Function from Activity-Dependent Ion Channel Regulation. Curr. Biol. *26*, 2935–2941.

83. Tang, L.S., Taylor, A.L., Rinberg, A., and Marder, E. (2012). Robustness of a rhythmic circuit to short- and long-term temperature changes. J. Neurosci. *32*, 10075–10085.

84. Zhurov, Y., and Brezina, V. (2005). Temperature compensation of neuromuscular modulation in aplysia. J. Neurophysiol. *94*, 3259–3277.

85. Belgacem, Y.H., and Borodinsky, L.N. (2015). Inversion of Sonic hedgehog action on its canonical pathway by electrical activity. Proc. Natl. Acad. Sci. USA *112*, 4140–4145.

86. Shim, S., Zheng, J.Q., and Ming, G.L. (2013). A critical role for STIM1 in filopodial calcium entry and axon guidance. Mol. Brain *6*, 51.

87. Saint-Jeannet, J.P. (2017). Whole-Mount In Situ Hybridization of Xenopus Embryos. Cold Spring Harb. Protocol. Published online October 30, 2017. https://doi.org/10.1101/pdb.prot097287.

88. Balashova, O.A., Visina, O., and Borodinsky, L.N. (2017). Folate receptor 1 is necessary for neural plate cell apical constriction during *Xenopus* neural tube formation. Development *144*, 1518–1530.

89. Eisen, J.S., and Smith, J.C. (2008). Controlling morpholino experiments: don't stop making antisense. Development *135*, 1735–1743.

STAR★METHODS

KEY RESOURCES TABLE

REAGENT or RESOURCE	SOURCE	IDENTIFIER
Antibodies		
Mouse monoclonal anti-HB9	Developmental Studies Hybridoma Bank	Cat# 81.5C10; RRID:AB_2145209
Rabbit polyclonal anti-TRPM8 (extracellular)	Alomone Labs	Cat# ACC-049; RRID:AB_2040254
Mouse monoclonal anti-NCAM	Developmental Studies Hybridoma Bank	Cat# 4d; RRID:AB_528389
Mouse monoclonal anti-HNK-1	Sigma-Aldrich	Cat# C6680; RRID:AB_1078474
Mouse monoconal anti-beta-tubulin	Developmental Studies Hybridoma Bank	Cat# E7; RRID:AB_528499
Mouse monoclonal anti-neurofilament associated protein	Developmental Studies Hybridoma Bank	Cat# 3A10; RRID:AB_531874
Sheep polyclonal anti-Digoxigenin-AP, Fab fragments	Roche	Cat# 11093274910; RRID:AB_514497
Chemicals, Peptides, and Recombinant Proteins		
Alexa Fluor 488-Dextran conjugate	Invitrogen	D22910
N-(3-Aminopropyl)-2-[(3-methylphenyl)methoxy]-N-(2-thienylmethyl) benzamide hydrochloride (AMTB), TRPM8 inhibitor	Tocris	3989
(-)-menthol, TRPM8 agonist	Selleckchem.com	S4714
Veratridine, voltage-gated sodium channel agonist	Sigma-Aldrich	V5754
Calcicludine, voltage-gated calcium channel blocker	Alomone Labs	SPC-650
ω-conotoxin GVIA, N-type calcium channel blocker	Sigma-Aldrich	C9915
Flunarizine, T-type calcium channel blocker	Sigma-Aldrich	F8257
Tetrodotoxin, voltage-gated sodium channel blocker	Sigma-Aldrich	T8024
Tricaine Methanesulfonate (MS-222)	Western Chemical	TRS1
Fluo-4, AM	Thermo Fisher Scientific	F14201
Critical Commercial Assays		
Apoptag-Fluorescein *In Situ* Apoptosis Detection Kit	Millipore	S7110
Dual Luciferase Reporter Assay System	Promega	E1910
MMLV Reverse Transcriptase 1st-Strand cDNA Synthesis Kit	Lucigen	MM070150
SV Total RNA Isolation System	Promega	Z3100
mMESSAGE mMACHINE T7 Transcription Kit	Ambion/ThermoFisher	AM1344
mMESSAGE mMACHINE SP6 Transcription Kit	Ambion/ThermoFisher	AM1340
Experimental Models: Organisms/Strains		
Xenopus laevis, adult females and males	Nasco	LM00531 and LM00715
Oligonucleotides		
RT-PCR primer sequence *Xenopus laevis trpm8*: forward GAGGATGTACACTTGCTGCG; reverse TGCCTCTACTGCCATTTCCA	This paper	N/A
RT-PCR primer sequence *Xenopus laevis odc*: forward: GCCATTGTGAAGACTCTCTCCATT; reverse: ATCCGCTCGGGGGGAAACTCC	This paper	N/A

Continued

REAGENT or RESOURCE	SOURCE	IDENTIFIER
In situ trpm8 probe: GAGCTCTAGGACTCTCTACTCAAGTTTCTCACG AAGCATCGAGTTGTCCCTGGATGAGATAGATGCTGGCAAATTCAT TCAAGAAAACTTCAAGAAGAGAGAATGCGTGACATACACAAAAGA TCCCAGGTCACCGGAGGGTGTCTGCAAATGTGGATATTCCCGGAG CCAGCACACTGAAGGCATACAGAGCAACCAGAATGAGAAGTGGA ACTACAAGAAGAACACAAAAGATCTGCCCACAGATGCCTATGGGG ATATCCAGTTTGAAACCTTTGGAAGAAGAGGAAAGTACATTCGCCT GTCCCGAGAAACTACTCCTGAAATTCTGTATGAGCTGATGACCAAA TACTGGCAGCTGAAGACCCCAAACCTTATCATCTCTGTAACAGGA GGAGCCAAGAACTTCTCCCTGAAGCCACGAATGCGCAAAATCTTC AGCCGCCTCATTTACATTGCTCAGACCAAAGGAGCCTGGATATTC ACAGGAGGCACTCACTATGGTCTGATGAAGTACATTGGAGAAGTG GTCAGGGATAATACTATAAGCCAAAGCTCAGAAGAAAAAGTAATT GCTATTGGTATTACAGCTTGGGGAATGATCTCCAACCGAGAATCA CTGATTCGTAGCTCCAATAATGAGGGTAATTATGTTGCTCAGTATG TCATGGATGAGCAGAAGAGAGATCCACTATACTGCCTGGACAACA ACCACACTCATTTGATTCTTGTAGACAATGGCACCCATGG	This paper	N/A
trpm8 morpholinos	Gene Tools	N/A
TRPM8-sbMO: 5′TGACCCTCTATGTGCCTTACTATCT3′.		
TRPM8-tbMO1: 5′ATGGTCTGACAGTCATTGTAAAGCT3′.		
TRPM8-tbMO2: 5′CTGCTGACACCCTTTGTATCTCTAA3′.		
Control-MO: 5′CCTCTTACCTCAGTTACAATTTATA3′.		
Primer sequences for detecting TRPM8 knockdown: forward: 5′-ACAAAGGGTGTCAGCAGTGT-3′; reverse: 5′-CTCCGGT GACCTGGGATCTT-3′.	This paper	N/A
pMO-*trpm8*	[45]	N/A
rNav2αβ	[5]	N/A
hb9-270-luc	This paper	N/A
hb9-270-$^{CREB\_mut}$-luc	This paper	N/A
hb9-270-$^{AP1\_mut}$-luc	This paper	N/A
Software and Algorithms		
Imaris	Bitplane	Version 9.2
NIS Elements	Nikon	Version 4.20
Prism	Graphpad	Version 8.02
ImageJ	NIH	https://imagej.nih.gov/ij/
Other		
Bipolar temperature controller	Warner Instruments	CL-100
Quick Exchange heated/cooled platform	Warner Instruments	QE-1HC

CONTACT FOR REAGENT AND RESOURCE SHARING

Further information and requests for resources and reagents should be directed to and will be fulfilled by the Lead Contact, Laura Borodinsky (lnborodinsky@ucdavis.edu).

EXPERIMENTAL MODEL AND SUBJECT DETAILS

Frog embryo and larva growth conditions

Xenopus laevis adult frogs used for obtaining mature oocytes and testes for *in vitro* fertilization were housed in an animal facility of the University of California Davis, Sacramento, CA USA and were originally purchased from Nasco. Animal handling and procedures were approved by the Institutional Animal Care and Use Committee in accordance with the Animal Welfare Act and Policy on Humane Care and Use of Laboratory Animals, and met USA regulations.

Freshly laid eggs were fertilized *in vitro* with dissected testis in 10% Marc's Modified Ringer (MMR) solution (10mM NaCl, 0.2mM KCl, 0.1mM MgSO$_4$, 0.2mMCaCl$_2$, 0.5mM HEPES (pH 7.8), 0.01mM EDTA). Four to five hours post fertilization, cohorts of age-matched siblings were raised at one of four temperatures corresponding to cold (14.5 or 16°C) or warm (22.5 or 26.5°C) ranges

for this species, in 10% MMR in Petri dishes placed on a temperature gradient plate or in a cooler or incubator until the stage required for each experiment. Number of animals used for each experiment was determined by the minimal number necessary to assess statistical significance based on previous studies in which we performed comparable type of experiments, and through power analysis. Images of live, stage 40 larvae were collected on a Nikon AZ100 Stereoscope using a 0.5X objective. Larva length and axial muscular width were measured using NIS Elements software (Nikon). Embryo and larva gender were not determined since it is not a relevant variable for the current study. Nevertheless, both females and males were evenly included.

METHOD DETAILS

Sensorimotor behavior
Larvae were positioned in the center of a 35-mm dish filled with 10% MMR. The temperature of the dish was regulated during testing with a bipolar temperature controller (CL-100) and quick exchanged heated/cooled platform (QE-1HC, Warner Instruments). Larvae were tested at either cold or warm temperature (14.5 or 22.5 ± 0.5°C, respectively). A hand-held mounted eyebrow hair was used to lightly stroke the larva from the back of the head, along the side until the mid-tail of the resting larva, or until the larva swam away. Responses were video recorded at 30 Hz. Each larva was tested at least 20 times with at least 5 s rest period between trials. Six larvae from at least two independent sibling cohorts were tested per treatment group. Stage 37/38 and 40 larva responses were evaluated by an experimenter blind to the temperature treatment, and categorized by swimming away (swim), flexing to either side (flexion), or no response as described by Roberts and colleagues [26, 27]. Swimming responses for stage 40 larvae were traced and analyzed using NIS Elements software (Nikon).

Immunostaining
Stage 35 and 40 larvae were fixed with 4% paraformaldehyde (PFA) in phosphate-buffered saline (PBS, pH 7.4) for 2-3 h at 4°C, incubated in 5% sucrose for 10 min, then overnight in 30% sucrose at 4°C and embedded in OCT compound (Tissue-Tek, Thermo Fisher Scientific). Transverse, 10-μm-thick cryosections were collected over a region 400-800 μm caudal to the eye. This corresponds to the region between the 2nd and 4th post-otic vesicle inter-myotome cleft. Cryosections were permeabilized in 0.1% Triton X-100, incubated overnight at 4°C with primary antibodies for homeobox gene 9 (HB9, 1:10, Developmental Studies Hybridoma Bank), followed by 3-h incubation at 23°C with fluorescently-tagged secondary antibodies, and 10-min incubation with DAPI for nuclear staining. Images were collected using an Olympus IX71 epifluorescent microscope with 20X or 40X air objectives, or Nikon A1 confocal microscope with a 40X oil objective. Immunoreactive cells were counted in at least 20 consecutive sections per larva, and from at least 4 larvae per treatment.

Stage 23-26 embryos were fixed in 2.8% trichloroacetic acid, PBS, pH 7.4 for 1.5 h at 23°C, dehydrated in 70%, 90%, and 100% ethanol (2 min each), cleared in SafeClear for 10 min, and embedded in paraffin. Transverse, 10-μm-thick sections of spinal cord were collected. Samples were permeabilized in 0.1% Triton X-100, incubated in 1% BSA blocking solution for 1 h at 4°C, stained overnight at 4°C with primary antibody for TRPM8-extracellular (1:700-1:3000, Alomone Labs), and NCAM (1:500, Developmental Studies Hybridoma Bank), and incubated for 2 h at 23°C with secondary antibody. Images were collected using a Nikon A1 confocal microscope with 40X or 60X oil objectives.

Whole mount preparations were made from stage 40 larvae fixed in 4% PFA for 4 h at 4°C. Skin covering the axial musculature was removed and larvae were bleached in 1:2 Dent's fixative/H$_2$O$_2$ overnight at 23°C. Samples were washed and permeabilized in 0.5% Triton X-100, stained overnight at 4°C with primary antibody for HNK-1 (1:500, Sigma-Aldrich) and 3A10 (1:300, Developmental Studies Hybridoma Bank), followed by overnight staining with secondary antibody at 4°C, and finally cleared overnight in benzyl benzoate. Z stack images of the axial musculature were collected between the 3rd-7th stripes of muscle fibers, with the 1st being the most anterior muscle chevron, on a Nikon C1 confocal microscope using 20x air objective. Measurements of immunoreactive axons were performed in at least 10 larvae per treatment.

Retrograde labeling of motor neurons
Motor neurons were back filled with Alexa 488-dextran conjugate (Invitrogen). The fluorescent dextran was mixed with a small volume of distilled water and the viscous paste was loaded into the tip of a thin insect pin. Larvae grown at different temperatures were anesthetized with 0.1% MS222 and stabbed with the loaded needle through the skin and into the right ventral musculature. Larvae were kept in anesthetic for 15 min followed by washes with 10% MMR where they were allowed to recover for 2 h. Then larvae were anesthetized again and fixed with 2% glutaraldehyde in phosphate buffer for 30 min at room temperature. Fixed samples were dissected to expose the spinal cord by removing the skin and muscle on the right side. Exposed spinal cords were mounted in Vectashield mounting medium H1200 (Vector Labs) and confocally imaged with a 20X objective with a Nikon C2 microscope. Labeled cells were counted from at least 10 larvae per treatment.

TUNEL (Terminal deoxynucleotidyl transferase dUTP nick end labeling) assay
Apoptotic cells were labeled using the TUNEL (terminal deoxynucleotidyl transferase dUTP nick end labeling) assay in transverse sections of stage 40 spinal cord from samples fixed in 4% PFA, phosphate-buffered saline (pH 7.4) for 2 h at 4°C, dehydrated in 70%, then 90%, and finally 100% ethanol (5 min each), cleared in SafeClear for 10 min, and embedded in paraffin for sectioning. Staining was performed according to the Apoptag-Fluorescein In Situ Apoptosis Detection Kit (Cat # S7110, Millipore). Images

were collected using an Olympus IX71 epifluorescent microscope with 40X air objective. Immunoreactive cells were counted in at least 20 consecutive sections per larva, and from at least 4 larvae per treatment.

Calcium imaging

For assessment of potential acute temperature-dependent changes in Ca^{2+} spike activity in the embryonic spinal cord, the ventral surface was exposed in stage 22-24 embryos grown at 22.5°C, the most common temperature in which embryos are grown in the lab. Samples were incubated with 0.5 μM Fluo-4 acetoxymethyl ester (Fluo-4-AM, Molecular Probes), cell-permeant Ca^{2+}-sensitive dye, for 1 h at 23°C. Images were acquired at 0.2 Hz during 1 to 3, 30-min periods, using a Nikon Swept-field confocal microscope. Ca^{2+} transients were traced with the imaging software NIS Elements (Nikon). Ca^{2+} spikes were counted when transients reach their peak within 5 s, and the peak amplitude is more than twice the standard deviation of the noise in fluorescence intensity. Acute changes in temperature during imaging were implemented with a bipolar temperature controller (CL-100) and quick exchanged heated/cooled platform (QE-1HC, Warner Instruments) in a random order. Ca^{2+} activity was imaged in ventral spinal cord from at least 3 embryos per treatment.

For TRPM8 inhibition experiments, samples were incubated with 10 μM N-(3-Aminopropyl)-2-[(3-methylphenyl)methoxy]-N-(2-thienylmethyl)benzamide hydrochloride (AMTB, Tocris) or 0.1% DMSO (vehicle control) for 20 min prior to imaging. For TRPM8 pharmacological activation experiments, exposed ventral spinal cord from embryos was loaded with Fluo4-AM and imaged at 1 Hz for approximately 30 s when 100 μM (-)-menthol (Selleckchem) was bath applied and imaged for another 60 s. Detection of $[Ca^{2+}]$ changes in response to menthol was done by tracing with the imaging software NIS Elements (Nikon) as described above. Control experiments consisted in adding 0.05% DMSO (vehicle) instead of (-)-menthol to the same sample.

Manipulation of spontaneous Ca^{2+} activity

Spontaneous Ca^{2+} activity in the developing spinal cord was modified using both pharmacological and genetic approaches. For pharmacological manipulation of spontaneous Ca^{2+} activity, agarose beads impregnated with 1 mM veratridine (voltage-gated Na^+ channel agonist, Sigma) or a cocktail of voltage-gated Ca^{2+} and Na^+ channel blockers (VGCblock; 200 nM calcicludine (Calbiochem), 10 μM ω-conotoxin–GVIA, 10 μM flunarizine, and 10 μg/ml tetrodotoxin (Sigma)) were implanted at stage 17-18. For genetic manipulation of spontaneous Ca^{2+} activity, $rNa_v2\alpha\beta$ (Na_v2a, 100 pg $rNa_v2a\alpha$ and 500 pg $rNa_v2a\beta$ mRNA) was bilaterally injected at the two-cell stage. Embryos were grown at room temperature until stage 35-36 when samples were collected and processed for immunostaining with anti-HB9 (Developmental Studies Hybridoma Bank) as described above in Immunostaining. Immunoreactive cells were counted in at least 20 consecutive sections per larva, and from at least 4 larvae per treatment.

Luciferase Assay

Using the ECR Browser we found two potential activity-responsive elements (CRE-like and AP1) in the 5′ regulatory region of the human *HB9* gene in the conserved M250 region, also known as region B. A wild-type or mutant 270 bp fragment containing these activity-wild-type or mutated responsive elements, respectively, were sub-cloned and placed directly upstream of a gene coding for the firefly luciferase. Firefly luciferase constructs along with the normalizing CMV enhancer-controlled renilla luciferase construct were injected in two-cell stage wild-type and $rNa_v2a\alpha\beta$ (Nav2a, coinjected with 100 pg $rNa_v2a\alpha$ and 500 pg $rNa_v2a\beta$ mRNA)-over-expressing embryos. Spinal cords from stage 24 embryos were dissected and incubated with drugs or vehicle for 8 h followed by processing for luciferase assay reading [85]. Concentrations of drugs used were the following: 1 μM veratridine (voltage-gated Na^+ channel agonist, Sigma); VGCblock: 20 nM calcicludine (Calbiochem), 1 μM ω-conotoxin–GVIA, 1 μM flunarizine, and 1 μg/mL tetrodotoxin (Sigma). Samples were homogenized in 20 μL of passive lysis buffer (Dual-Luciferase Reporter Assay System, Promega). Firefly and renilla luciferase activities were quantified using a Microbeta Trilux luminescence counter (Perkin-Elmer) after addition of the LARII and Stop&Glow reagents, respectively (Dual-Luciferase Reporter Assay System, Promega). Firefly/renilla activity ratio was then calculated for each sample from at least 5 spinal cords per treatment.

RT-PCR

RT-PCR was performed on cDNA synthesized (MMLV Reverse Transcriptase 1st-Strand cDNA Synthesis Kit, Epicenter) from stage 24 or 46 whole animal or spinal cord extracted mRNA (SV Total RNA Isolation System, Promega). Primers were designed to amplify sequences for *Xenopus laevis* transient receptor potential cation channel subfamily M member 8 (*trpm8*) and ornithine decarboxylase (*odc*, control). Primer sequences: *X. laevis* TRPM8 forward: GAGGATGTACACTTGCTGCG; reverse: TGCCTCTACTGCCATTTCCA. *X. laevis* ODC forward: GCCATTGTGAAGACTCTCTCCATT; reverse: ATCCGCTCGGGGGGAAACTCC. Samples were run in triplicate.

In situ hybridization

Whole-mount *in situ* hybridization was performed by using digoxigenin (DIG)-UTP-labeled RNA probe [86, 87] on stage 24 embryos. 750 bp of SacI/ NcoI digestion of RT-PCR product of *trpm8* was used for the specific anti-sense and sense probes after cloning into pGEMT-vector and transcribed *in vitro*. The labeled probes were detected with alkaline phosphatase (AP)-conjugated anti-DIG antibody (Fab fragments, Roche) and visualized with the BM-purple AP substrate. At least 5 embryos were processed for anti-sense and sense probing.

Western blot assays

Unfertilized eggs, stage 24 embryos or stage 40-41 larvae were snap-frozen for western blot assays. Samples (1-3 replicates per treatment; 10 eggs per replicate, 8 stage 24 embryos per replicate, or 2 stage 40-41 larvae per replicate) were homogenized on ice in homogenization buffer (25 mM HEPES (pH 7.4), 5 mM EDTA, protease inhibitors cocktail (Thermo Fisher Scientific) then centrifuged for 10 min at 16,000 g, and pellet discarded. Supernatant was collected and mixed with 2x protein loading buffer (125 mM Tris-HCl, pH 6.8, 4% SDS, 20% (w/v) glycerol, 0.005% Bromophenol Blue) then boiled for 2 min. Lysates were loaded on 8% SDS-page gel and samples were transferred to PVDF membrane [88]. Immunoblotting was performed overnight with anti-TRPM8 rabbit polyclonal affinity-purified antibody (1:500-1:700 in 5% milk) raised against the peptide SDVDGTTYDFAHC, corresponding to the amino acid residues 917-929 in the 3rd extracellular loop of human TRPM8 (Alomone Labs), which is conserved (11 out of 13 residues) in *Xenopus laevis* TRPM8. This was followed by incubation with horseradish peroxidase (HRP)-conjugated secondary antibody (Jackson ImmunoResearch; 1:10,000) and visualized using Western Lightning Plus-ECL, Enhanced Chemiluminescence Substrate (Perkin Elmer). For protein loading control, PVDF membranes were stripped in stripping buffer (0.2 M glycine-HCl buffer, pH 2.5, 0.05% Tween) for 20 min then re-probed overnight with anti-β-tubulin mouse monoclonal antibody (1:50 in 5% milk, Developmental Studies Hybridoma Bank), followed by HRP-conjugated secondary antibody (Jackson ImmunoResearch; 1:10,000) and visualized as described above.

TRPM8 knockdown

Embryos were injected at the 2-cell stage with 2.5-5 pmol of a splicing-blocking morpholino oligonucleotide targeting exon2-intron-exon3 of *Xenopus laevis trpm8* pre-mRNA (TRPM8-sbMO), two non-overlapping xlTRPM8 translation-blocking morpholino (TRPM8-tbMO1 and 2) or standard control morpholino (Control-MO, Gene Tools, LLC). TRPM8-sbMO: 5′-TGACCCTCTATGTGCCTTAC TATCT-3′. Primer sequences for detecting TRPM8 knockdown: forward: 5′-ACAAAGGGTGTCAGCAGTGT-3′; reverse: 5′-CTCC GGTGACCTGGGATCTT-3′. TRPM8-tbMO1: 5′-ATGGTCTGACAGTCATTGTAAAGCT-3′. TRPM8-tbMO2: 5′-CTGCTGACACCCTTT GTATCTCTAA-3′. Control-MO: 5′-CCTCTTACCTCAGTTACAATTTATA-3′. Four to five h post-injection, embryos were grown at cold (16°C and not 14.5°C to avoid morpholino binding to non-specific mRNA [89]) or warm (22.5°C) temperature until the stage required for each experiment.

Efficiency of knockdown was assessed by RT-PCR or western blot assays (repeated 3x for each tbMO) when embryos were injected with TRPM8-sbMO or TRPM8-tbMO, respectively. Overall gross development of TRPM8-MO-injected embryos was comparable to Control-MO-injected siblings, albeit slightly delayed. Nevertheless, developmental stages used for each assay were always equalized between control and experimental samples.

Transverse sections of stage 40 spinal cord from TRPM8-sbMO and Control-MO larvae were fixed in 4% PFA, phosphate-buffered saline (pH 7.4) for 2 h at 4°C, dehydrated in 70%, then 90%, and finally 100% ethanol (5 min each), cleared in SafeClear for 10 min, and embedded in paraffin for sectioning. Sections were immunostained with anti-HB9 (Developmental Studies Hybridoma Bank) and imaged as described above in Immunostaining. Immunoreactive cells were counted in at least 20 consecutive sections per larva, and from 5 larvae per treatment.

TRPM8 overexpression

Xenopus laevis trpm8 mRNA was *in vitro* transcribed (mMessage mMachine T7 kit, Ambion/Thermo Fisher Scientific) from the linearized cDNA template obtained from the construct pMO-*trpm8*, generous gift from the Julius lab [45]. Five hundred pg of *trpm8* mRNA were injected per blastomere in 2-cell stage embryos. Bilaterally injected stage 26 embryos were processed for western blot assays and unilaterally injected embryos for frozen transverse section immunostaining followed by confocal imaging as described above.

QUANTIFICATION AND STATISTICAL ANALYSIS

Statistical analysis

Statistical tests were performed with GraphPad Prism statistical software (Version 8.0.2). Sample sizes were determined based on previous studies [4, 5, 85, 88] and through power analysis, and indicated for each experiment in figure legends. Datasets were evaluated for normality using the Shapiro-Wilk test. For normally distributed data, mean ± SEM are reported, and datasets compared using two-tailed unpaired or paired t tests, 1-way ANOVA, 2-way ANOVA, or repeated-measures mixed-effects analysis with post hoc Tukey test depending on experimental design. For non-normally distributed data, geometric means are reported, and datasets were either transformed for statistical comparison or compared using Wilcoxon matched-pairs signed rank test, Kolmogorov-Smirnov two-tailed test, or Kruskal-Wallis test with Dunn's multiple comparison depending on experimental design. Statistical tests used for each experiment are indicated in corresponding figure legends. Differences were considered significant when $p < 0.05$.